

PREPARED FOR SUBMISSION TO JHEP

# Electroweak symmetry breaking in the inverse seesaw mechanism

---

Sanjoy Mandal,<sup>a</sup> Rahul Srivastava,<sup>b</sup> José W. F. Valle<sup>a</sup>

<sup>a</sup>*AHEP Group, Institut de Física Corpuscular – CSIC/Universitat de València, Parc Científic de Paterna.*

*C/ Catedrático José Beltrán, 2 E-46980 Paterna (Valencia) - SPAIN*

<sup>b</sup>*Department of Physics, Indian Institute of Science Education and Research - Bhopal  
Bhopal Bypass Road, Bhauri, Bhopal, India*

*E-mail:* [smandal@ific.uv.es](mailto:smandal@ific.uv.es), [rahul@iiserb.ac.in](mailto:rahul@iiserb.ac.in), [valle@ific.uv.es](mailto:valle@ific.uv.es)

**ABSTRACT:** We investigate the stability of Higgs potential in inverse seesaw models. We derive the full two-loop RGEs of the relevant parameters, such as the quartic Higgs self-coupling, taking thresholds into account. We find that for relatively large Yukawa couplings the Higgs quartic self-coupling goes negative well below the Standard Model instability scale  $\sim 10^{10}$  GeV. We show, however, that the “dynamical” inverse seesaw with spontaneous lepton number violation can lead to a completely consistent and stable Higgs vacuum up to the Planck scale.

---

## Contents

<b>1</b>	<b>Introduction</b>	<b>1</b>
<b>2</b>	<b>The Inverse Seesaw mechanism</b>	<b>4</b>
<b>3</b>	<b>Higgs vacuum stability in inverse seesaw</b>	<b>6</b>
3.1	Effective Theory	6
3.2	Full Theory	7
<b>4</b>	<b>The Majoron Completion of the inverse Seesaw</b>	<b>10</b>
<b>5</b>	<b>Vacuum stability in inverse seesaw with majoron</b>	<b>12</b>
5.1	Case I: $v_\sigma \gg v_\Phi$	12
5.2	Case II: $v_\sigma = \mathcal{O}(v_\Phi)$	14
<b>6</b>	<b>Comparing sequential and missing partner inverse seesaw</b>	<b>16</b>
6.1	Sequential versus missing partner seesaw: electroweak vacuum stability	16
6.2	Sequential versus missing partner seesaw: brief phenomenological discussion	17
<b>7</b>	<b>Impact of invisible Higgs decay on the vacuum stability</b>	<b>18</b>
<b>8</b>	<b>Conclusions</b>	<b>21</b>
<b>A</b>	<b>RGEs: Inverse seesaw</b>	<b>22</b>
A.1	Higgs quartic scalar self coupling	22
A.2	Yukawa Couplings	23
<b>B</b>	<b>RGEs: Inverse seesaw with majoron</b>	<b>23</b>
B.1	Quartic scalar couplings	23
B.2	Yukawa Couplings	24

---

## 1 Introduction

The historical discovery of the Higgs boson [1, 2] and the subsequent precise measurements of its properties [3] can be used to shed light on the electroweak symmetry breaking mechanism. In particular, we can now not only determine the value of the quartic coupling of the Standard Model scalar potential at the electroweak scale, but also use it to shed light on possible new physics all the way up to Planck scale. Given the present measured top quark

and Higgs boson masses, one can calculate the corresponding Yukawa  $y_t$  and Higgs quartic  $\lambda_{\text{SM}}$  couplings within the Standard Model. These, along with the  $\text{SU}(3)_c \otimes \text{SU}(2)_L \otimes \text{U}(1)_Y$  gauge couplings  $g_1, g_2, g_3$  respectively, are the most important input parameters characterizing the Standard Model renormalization group equations (RGEs). Given the values of these input parameters<sup>1</sup>, as shown in Table 1, the Higgs quartic coupling tends to run negative between the electroweak and Planck scales, as seen in Fig. 1.

	$g_1$	$g_2$	$g_3$	$y_t$	$\lambda_{\text{SM}}$
$\mu(m_t)$	0.462607	0.647737	1.16541	0.93519	0.126115

**Table 1.**  $\overline{\text{MS}}$  values of the input parameters at the top quark mass scale,  $\mu(m_t) = 173 \pm 0.4$  GeV [3].

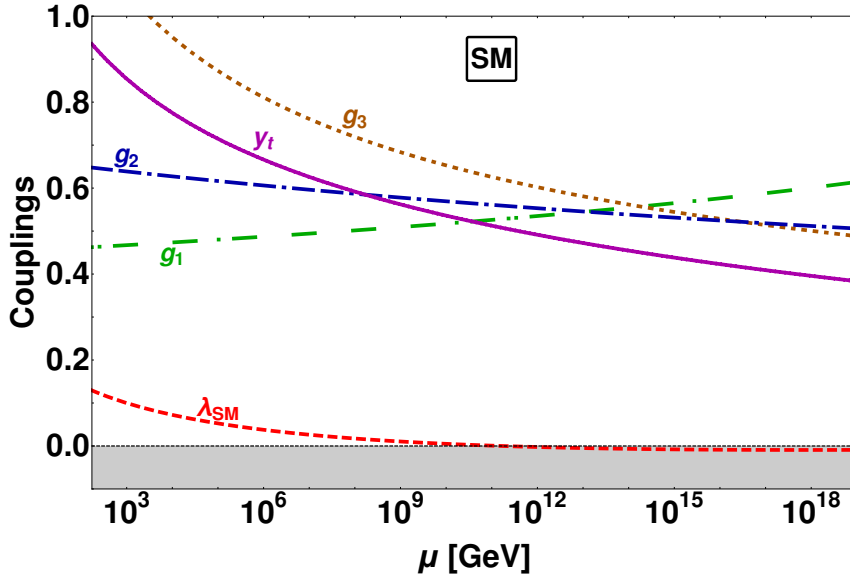


**Figure 1.** The renormalization group evolution of the Standard Model gauge couplings  $g_1, g_2, g_3$ , the top quark Yukawa coupling  $y_t$  and the quartic Higgs boson self-coupling  $\lambda_{\text{SM}}$ . Here we adopt the  $\overline{\text{MS}}$  scheme, taking the parameter values at low scale as input, see [5] for details.

One sees that the Standard Model Higgs quartic coupling  $\lambda_{\text{SM}}$  becomes negative at an energy scale  $\sim 10^{10}$  GeV. This would imply that the Standard Model Higgs potential is unbounded from below. Hence, the Standard Model vacuum is not absolutely stable [4, 6, 7]. Instead, these next-to-next-to-leading order analyses of the Standard Model Higgs potential suggest that the vacuum is actually metastable.

Moreover, despite its many successes, the Standard Model cannot be the final theory of nature. One of its main shortcomings is its inability to account for neutrino mass generation, needed to describe neutrino oscillations [8]. The Higgs vacuum stability problem

<sup>1</sup>The numbers given in Table 1 are the central values. We use them as the input parameters for our RGEs. The importance of errors has been studied in Ref. [4], to which we refer the reader for more details.

in neutrino mass models can become worse than in the Standard Model [9–16]. Here we follow Ref. [5] and confine ourselves to the Standard-Model-based seesaw mechanism using the simplest  $SU(3)_c \otimes SU(2)_L \otimes U(1)_Y$  gauge group.

The latter can be realized in “high-scale” schemes with explicit [17] or spontaneous violation of lepton number [18, 19]. These typically involve messenger masses much larger than the electroweak scale. Alternatively, neutrino mass may result from “low-scale” physics [20]. For example, the type-I seesaw mechanism can be mediated by “low-scale” messengers. This happens in the inverse seesaw mechanism. Lepton number is broken by introducing extra  $SU(3)_c \otimes SU(2)_L \otimes U(1)_Y$  singlet fermions with small Majorana mass terms, in addition to the conventional “right-handed” neutrinos. Again, one can have either explicit [21] or spontaneous lepton number violation [22].

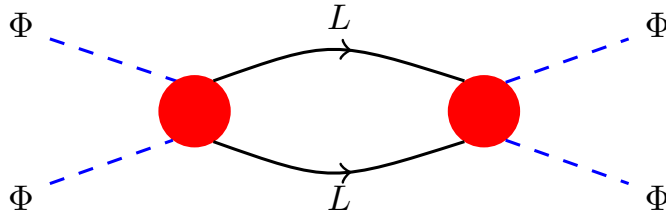


**Figure 2.** Destabilizing effect of Weinberg’s effective operator on the Higgs quartic interaction.

Any theory with massive neutrinos has an intrinsic effect, illustrated in Fig. 2, that may potentially destabilize the electroweak vacuum <sup>2</sup>. This vacuum stability problem becomes severe in low-scale-seesaw schemes [5]. Indeed, if the heavy mediator neutrino lies in the TeV scale, its Yukawa coupling will run for much longer than in the high-scale type-I seesaw. As a consequence, the quartic coupling  $\lambda$  tends to become negative sooner, much before the Standard Model instability sets in.

Here we examine the consistency of the electroweak symmetry breaking vacuum within the inverse seesaw mechanism. Apart from the destabilizing effect illustrated in Fig. 2 there will in general be other, model-dependent, and possibly leading contributions that can reverse this trend. We note that the spontaneous violation of lepton number, implying the existence of a physical Nambu-Goldstone boson, dubbed majoron [18, 19], can substantially improve the electroweak vacuum stability properties. Indeed, the extended scalar sector of low-scale-majoron-seesaw schemes plays a key role in improving their vacuum stability. This sharpens the results presented in Ref. [11]. Indeed, we find that renormalization group (RG) evolution can cure the vacuum stability problem in inverse seesaw models also in the presence of threshold effects. These can be associated both with the scalar as well

<sup>2</sup>In the presence of very specific symmetries this model-independent argument might be circumvented.

as the fermion sector of the theory <sup>3</sup>.

The paper is organized as follows. In Section 2, we describe neutrino mass generation in the inverse-seesaw model. In Section 3 we show that the vacuum stability problem becomes worse within the simplest inverse-seesaw extensions with explicitly broken lepton number. In Section 4, we then focus on the majoron completion of the inverse seesaw. We then show in Section 5 how the majoron helps stabilize the Higgs vacuum, all the way up to Planck scale. In Section 6, we compare the vacuum stability properties of the various missing-partner-inverse-seesaw variants with those of the sequential case. In Sec. 7 we briefly illustrate the interplay between vacuum stability and the restrictions on the Higgs boson invisible decays [23] that follow from current LHC experiments. Finally, we conclude and summarize our main results in Section 8.

## 2 The Inverse Seesaw mechanism

The issue of vacuum stability must be studied on a model-by-model basis. In this work we examine it in the context of inverse-seesaw extensions of the Standard Model. The inverse seesaw mechanism is realized by adding two sets of electroweak singlet “left-handed” fermions  $\nu_i^c$  and  $S_i$  [21, 22]. The relevant part of the Lagrangian is given by

$$-\mathcal{L} = \sum_{ij} Y_\nu^{ij} L_i \tilde{\Phi} \nu_j^c + M^{ij} \nu_i^c S_j + \frac{1}{2} \mu_S^{ij} S_i S_j + \text{H.c.} \quad (2.1)$$

where  $L_i = (\nu \ell)^T$ ;  $i = 1, 2, 3$  are the lepton doublets,  $\Phi$  is the Standard Model Higgs doublet,  $M$  is the Dirac mass term. The two sets of fields  $\nu^c$  and  $S$  transform under the lepton number symmetry  $U(1)_L$  as  $\nu^c \sim -1$  and  $S \sim +1$ , respectively. The  $M$  and  $\mu_S$  terms are both gauge invariant mass matrices, but only  $M$  is invariant under lepton number symmetry, since  $\mu_S$  violates lepton number by two units. Light neutrino masses are generated through the tiny lepton number violation. Indeed, after electroweak symmetry breaking, the effective light neutrino mass matrix has the following form

$$\mathcal{M}_\nu = \begin{pmatrix} 0 & m_D & 0 \\ m_D^T & 0 & M \\ 0 & M^T & \mu_S \end{pmatrix}, \quad (2.2)$$

with  $m_D = \frac{v}{\sqrt{2}} Y_\nu$ . Neutrino masses arise by block-diagonalizing Eq. 2.2 as,

$$\mathcal{U}^T \mathcal{M}_\nu \mathcal{U} = \mathcal{M}_D \quad (2.3)$$

through the unitary transformation matrix  $\mathcal{U}$ , where  $\mathcal{M}_D$  has a block-diagonal form. Since the lepton number is restored as  $\mu_S \rightarrow 0$ , the symmetry breaking entries of  $\mu_S$  can be made

---

<sup>3</sup>Notice that, while Ref. [5] included threshold effects, in the high-scale seesaw framework such effects appear only at high energies, and do not affect low-scale physics.

naturally small in the sense of t’Hooft. Apart from symmetry protection, the smallness of  $\mu_S$  may also result from having a radiative origin associated to new physics such as supersymmetry, left-right symmetry or dark matter physics [24–26]. In contrast, being gauge and lepton-number invariant, the elements of  $M$  are expected to be naturally large. Thus we obtain the hierarchy  $M \gg m_D \gg \mu_S$ . Under this hierarchy assumption we perform the standard seesaw diagonalization procedure [19], to obtain the effective light neutrino mass matrix  $m_\nu$  as

$$m_\nu \approx m_D M^{-1} \mu_S (M^T)^{-1} m_D^T = \frac{v^2}{2} Y_\nu M^{-1} \mu_S (M^T)^{-1} Y_\nu^T \quad (2.4)$$

Furthermore, in contrast to conventional type-I seesaw, the scale of lepton number violating parameter  $\mu_S$  is much smaller than the characteristic mediators scale  $M$ . As a result, the heavy singlet neutrinos become quasi-Dirac-type fermions<sup>4</sup>. Note that, the small lepton number violating Majorana mass parameters in  $\mu_S$  control the smallness of light neutrino masses. As  $\mu_S \rightarrow 0$ , the global lepton number symmetry is restored, and as a result, all the three light neutrinos are strictly massless. Small neutrino masses are “symmetry-protected” by the tiny value of  $\mu_S \neq 0$ . The smallness of  $\mu_S$  allows the Yukawa couplings  $Y_\nu$  to be sizeable, even when the messenger mass scale  $M$  lies in the TeV scale, without conflicting with the observed smallness of neutrino masses.

In contrast to the high-scale type-I seesaw, in inverse-seesaw schemes one can have a very rich phenomenology that makes them potentially testable in current or upcoming experiments. For example, the mediators would be accessible to high-energy collider experiments [28–31], with stringent bounds, e.g. from the Delphi and L3 collaborations [29, 30]. Moreover, they would induce lepton flavour and leptonic CP violating processes with potentially large rates, unsuppressed by the small neutrino masses [32–36]. Finally, since the mediators would not take part in low-energy weak processes, the light-neutrino mixing matrix describing oscillations would be effectively non-unitary [37–41]. In short, in contrast to the conventional high-scale seesaw, the inverse seesaw mechanism could harbor a rich plethora of accessible new physics processes, that could be just around the corner.

As  $\nu^c$  and  $S$ ’s are Standard Model gauge singlets, carrying no anomalies, there is no theoretical limit on their multiplicity. Many possibilities can arise depending on the number of  $\nu^c$  and  $S$  in a given model. In the sequential inverse seesaw model the number of  $\nu^c$  matches that of  $S$ , and there are three “heavy” quasi-Dirac leptons in addition to the three light neutrinos. For the case of different number of  $\nu^c$  and  $S$ , in addition to the light and heavy neutrinos, the spectrum will also contain intermediate states with mass proportional to  $\mu_S$ . These could be warm dark matter candidate if their mass lies in KeV scale [42].

For the sake of simplicity, here we consider only the case where  $\nu^c$  and  $S$  come with the same multiplicity. Moreover, since adding more fermion species will only worsen the Higgs

---

<sup>4</sup>The concept of quasi-Dirac fermions was first suggested for the light neutrinos in [27]. It constitutes a common feature of all low-scale seesaw models.

vacuum stability problem, in section 3 we opt for the minimal (3,1,1) case, namely a single pair of lepton mediators. In such minimal “missing-partner” seesaw [17] two of the light neutrinos will be left massless. In Section 6 we examine the quantitative differences between the different multiplicity choices concerning the issue of vacuum stability. Moreover, we briefly discuss the phenomenological viability of the various options.

### 3 Higgs vacuum stability in inverse seesaw

In the above preliminary considerations we have briefly summarized the main features of the inverse seesaw model. We now examine the effect of the new fermions  $\nu^c$  and  $S$  upon the stability of the electroweak Higgs vacuum. We take into account the effect of the thresholds associated with the extra fermions  $\nu^c$  and  $S$ , as well as the scalars (in Section 4 and 5) responsible for the spontaneous breaking of lepton number.

#### 3.1 Effective Theory

To begin with, in the effective theory where the heavy singlet fermions  $\nu^c$  and  $S$  are integrated out we have a natural threshold scale  $\Lambda \approx M$  given by their mass, see Eq. (2.1). As a result, below this scale the theory is the Standard Model plus an effective dimension five Weinberg operator [43], given by

$$-\mathcal{L}_\nu^{d=5} = \frac{\kappa}{2} L L \Phi \Phi + \text{H.c.} \quad (3.1)$$

where  $\kappa = (Y_\nu M^{-1} \mu_S (M^T)^{-1} Y_\nu^T)$  is the  $3 \times 3$  effective coupling matrix. Unless they are needed, in what follows we will suppress the generation indices. Note that  $\kappa$  has negative mass dimension. The above Lagrangian leads to a left-handed neutrino Majorana mass matrix as

$$m_\nu \equiv \kappa \frac{v^2}{2} \quad (3.2)$$

As a result, below the scale  $\Lambda$ , only the Standard Model couplings and  $\kappa$  will run. Neglecting lepton and light quark Yukawa couplings, the one-loop RGEs [44–46] are given by [5]

$$16\pi^2 \beta_\kappa = 6y_t^2 \kappa - 3g_2^2 \kappa + \lambda_\kappa \kappa \quad (3.3)$$

Due to the large top Yukawa coupling,  $\kappa$  slowly increases with the threshold scale  $\Lambda$ . We denote the Higgs quartic coupling in this case as  $\lambda_\kappa$  to distinguish it from the pure Standard Model case. The above Weinberg operator also gives a correction to the Higgs quartic coupling  $\lambda_\kappa$  below the scale  $\Lambda$ . The contribution of the coupling  $\kappa$  to the running of  $\lambda_\kappa$  is of order  $v^2 \kappa^2$  and thus negligible, as shown in [5, 14, 46]. Hence, below the scale  $\Lambda$ , the evolution of  $\lambda_\kappa$  will be almost the same as in the Standard Model.

### 3.2 Full Theory

We now turn to the region above the threshold scale  $\Lambda$ . In this regime we have the full Ultra-Violet (UV) complete theory. Hence one must take into account the RGEs of all the new couplings present in the model, as they will affect the evolution of the Higgs quartic coupling. In particular, we will see that the stability of the electroweak vacuum limits how large the Yukawa coupling  $Y_\nu$  can be. The Higgs quartic self-coupling in full UV-complete theory will be denoted by  $\lambda$ , to distinguish it from the Standard Model coupling  $\lambda_{\text{SM}}$  and from the effective theory quartic coupling  $\lambda_\kappa$  discussed above.

For simplicity we will first study the case of just one species of  $\nu^c$  and  $S$ , which we call the  $(3, 1, 1)$  inverse seesaw. As mentioned, this of course is not – by itself – realistic, as in this case only one of the light neutrinos obtains mass. However, the missing mass parameter may arise from a different mechanism [26] associated, say, with dark matter. Moreover, the  $(3, 1, 1)$  case provides the simplest reference scheme, that brings out all the relevant features. In Section 6 we will compare with the  $(3, 2, 2)$  and the  $(3, 3, 3)$  – the sequential inverse seesaw mechanism – with two and three species of  $\nu^c$  and  $S$ , respectively.

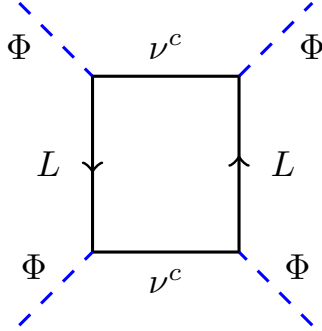


**Figure 3.** The destabilizing effect of right-handed neutrinos on the evolution of the Higgs quartic coupling.

The running of  $Y_\nu$  above the threshold scale is governed by the RGEs given in Appendix A. Apart from the RG evolution, one must also take into account the threshold corrections, associated with integrating the heavy fermions in the effective theory. The tree-level Higgs potential is given by

$$V = -\mu_\Phi^2(\Phi^\dagger\Phi) + \lambda(\Phi^\dagger\Phi)^2 \quad (3.4)$$

This will get corrections from higher loop diagrams of Standard Model particles as well as from the extra fermions present in the inverse seesaw model. It introduces a threshold correction to the Higgs quartic coupling  $\lambda$  at  $\Lambda = M$ . Here we follow Ref. [5] in estimating this threshold correction as  $\Delta\lambda_{\text{TH}} = -\frac{5}{32\pi^2}|Y_\nu|^4$ . We take into consideration this shift in  $\lambda$



at  $\Lambda = M$  when solving the RGEs,

$$\lambda(\Lambda) \rightarrow \lambda(\Lambda) - \frac{5}{32\pi^2} |Y_\nu|^4. \quad (3.5)$$

Having set up our basic scheme, let us start by looking at the impact of the Yukawa coupling  $Y_\nu$  on the stability of the Higgs vacuum. As already discussed, in the Standard Model, the running of the Higgs quartic coupling  $\lambda_{\text{SM}}$  is dominated by the top quark Yukawa coupling and becomes negative around energy scale  $\sim 10^{10}$  GeV. However, within the inverse seesaw, the Yukawa coupling  $Y_\nu$  in Eq.(2.1) can dominate the evolution of  $\lambda$  above the threshold scale  $\Lambda = M$ , as seen in Fig. 4.

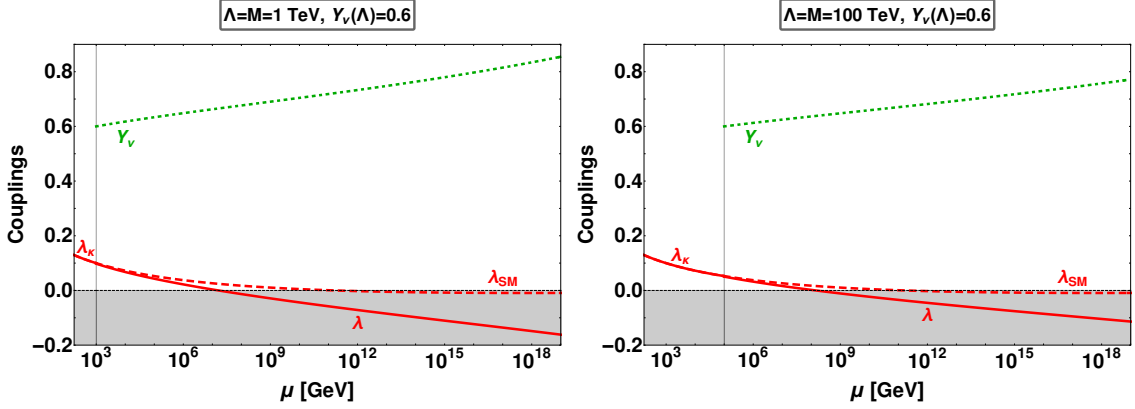


**Figure 4.** Evolution of the Higgs quartic self-coupling  $\lambda$  (solid-red) and Yukawa coupling  $Y_\nu$  (dotted-green) within the minimal (3,1,1) inverse seesaw scheme.  $\lambda_\kappa$  is the quartic coupling in the effective theory with the Weinberg operator. For comparison, we also plot the running of  $\lambda_{\text{SM}}$ , the SM quartic coupling, indicated by the dashed-red line.

In Fig. 4 we have shown the RG evolution of the relevant coupling parameters assuming the Yukawa coupling  $Y_\nu = 0.6$  at the threshold scale, taken to be  $\Lambda = M = 10^3$  GeV (left panel) and  $10^5$  GeV (right panel). We see that  $\lambda$  becomes negative at around energy scales  $3.27 \times 10^7$  GeV and  $3.16 \times 10^8$  GeV for the threshold scale  $\Lambda = 10^3$  GeV and  $10^5$  GeV, respectively. By comparing this with the running of the Standard Model Higgs quartic coupling  $\lambda_{\text{SM}}$  (red dashed), one sees how the Higgs vacuum stability problem becomes more acute in the inverse seesaw model. This was expected, since the new fermions tend to destabilize the Higgs vacuum, as illustrated in Fig. 3. It should also be noted that in the effective theory regime the evolution of the quartic coupling  $\lambda_\kappa$  almost coincides with that of  $\lambda_{\text{SM}}$ , due to the negligible effect of the Weinberg operator on its running. Finally, note that all couplings in Fig. 4 remain within the perturbative region up to Planck scale.

### Consistency Restrictions

We now turn to the issue of the general self-consistency of the inverse seesaw mechanism. In order to ensure a perturbative and mathematically consistent model, the tree-level couplings must satisfy certain conditions, e.g. all of them should have a perturbative value,

and the potential should be bounded from below. However, once we take into account the quantum corrections, these conditions also get corrected. In this section we analyze these modified conditions in more detail.

We start by examining the restrictions coming from perturbativity at tree-level, which require  $|Y_\nu| < \sqrt{4\pi}$ . The RG evolution of  $Y_\nu$  increases its value with increasing scale. Fig. 5 shows the evolution of  $Y_\nu$  and  $\lambda$ . From the left panel of Fig. 5 one sees that demanding that  $|Y_\nu| < \sqrt{4\pi}$  up to the Planck scale implies that  $|Y_\nu| \lesssim 0.8$  at the threshold scale  $\Lambda = 10^3$  GeV. However, as one can see from Fig. 5, the Higgs quartic coupling  $\lambda$  becomes negative much before the Planck scale. Therefore, demanding perturbativity of  $Y_\nu$  all the way up to the Planck scale does not ensure full consistency of the scalar potential. If one demands perturbativity only till, say, 100 TeV, as shown in right panel of Fig. 5, one finds that the perturbativity limit on  $Y_\nu$  is relaxed to  $|Y_\nu| \lesssim 2$  at the threshold scale  $\Lambda = 10^3$  GeV. Such large  $Y_\nu$  values lead to large threshold corrections for  $\lambda$  – the negative jump shown in the right panel – making it negative even before turning on its RG evolution.

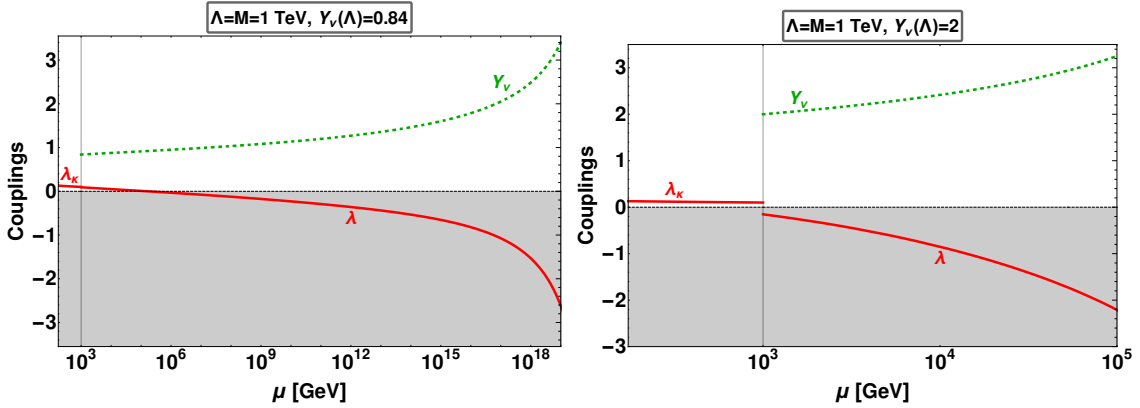


**Figure 5.** Perturbativity limits on the Yukawa coupling  $Y_\nu$ . The left panel requires  $Y_\nu < \sqrt{4\pi}$  up to the Planck scale, so that only RG evolution is relevant. The right panel demands  $Y_\nu < \sqrt{4\pi}$  only up to 100 TeV. In this case  $Y_\nu$  is large enough that threshold effects make  $\lambda$  negative even before running. In both cases the vacuum is unstable, i.e.  $\lambda < 0$ , before  $Y_\nu$  reaches the perturbative limit, see text for details.

This highlights the importance of taking into account the threshold corrections for  $\lambda$ . From Fig. 5 one sees that a large  $Y_\nu$  value can lead to an unbounded potential already at the threshold scale, even before RG evolution. Taking the Yukawa coupling  $Y_\nu(\Lambda) = 1.58$  at  $\Lambda = 10^3$  GeV makes  $\lambda(\Lambda) = 0$  due to threshold corrections. RG running will further decrease  $\lambda$  above the threshold scale, making the vacuum unstable. It is clear that threshold corrections are crucial when considering large Yukawa couplings and that a true limit on  $Y_\nu$  requires one to take into account both RG evolution as well as the threshold corrections it induces on the quartic coupling  $\lambda$ .

As an example, in Fig. 6 we show the result of demanding that neither  $Y_\nu$  goes non-

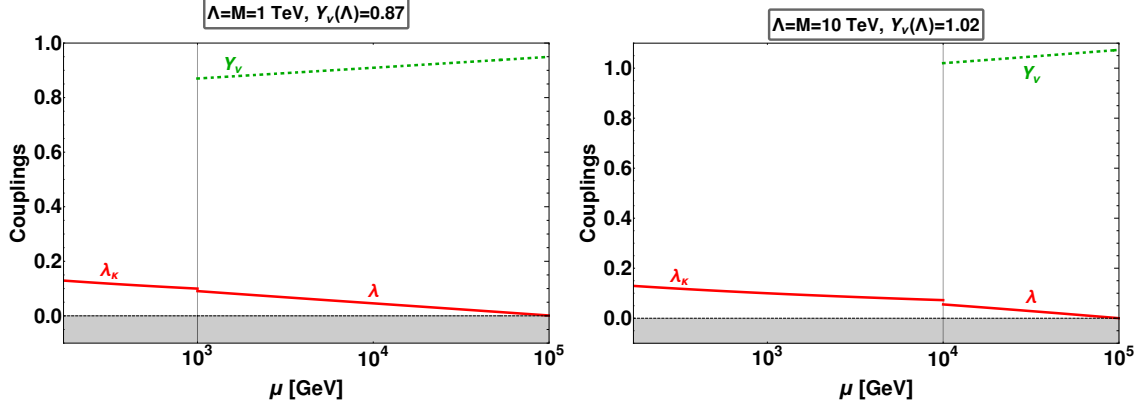


**Figure 6.** Limiting  $Y_\nu$  by demanding  $Y_\nu$  to remain perturbative and  $\lambda$  to remain positive up to 100 TeV. Left (right) panel correspond to threshold scales  $\Lambda = 1$  TeV ( $\Lambda = 10$  TeV). See text for details.

perturbative, nor  $\lambda$  goes negative up to 100 TeV. To quantify the implications of this demand, we have taken two threshold scales,  $\Lambda = 10^3 \text{ GeV}$  (left panel), and  $\Lambda = 10^4 \text{ GeV}$  (right panel), respectively. With this combined requirement we obtain the limit  $Y_\nu \lesssim 0.87$  (left panel) and  $Y_\nu \lesssim 1.02$  (right panel). This illustrates that the limit on  $Y_\nu$  also depends on the choices of threshold scale, for higher threshold scales the limit on  $Y_\nu$  gets relaxed.

#### 4 The Majoron Completion of the inverse Seesaw

In the previous section we saw that the addition of new fermions to the Standard Model in order to mediate neutrino mass generation via the inverse seesaw mechanism [21] has a destabilizing effect on the Higgs vacuum. This problem can be potentially cured if there are other particles in the theory providing a “positive” contribution to the RGEs governing the evolution of the Higgs quartic coupling. A well-motivated way to do this is to assume the dynamical version of the inverse seesaw mechanism [22].

Building up on the work of Ref. [11] here we focus on low-scale generation of neutrino mass through the inverse seesaw mechanism with spontaneous lepton number violation. Lepton number is promoted to a spontaneously broken symmetry within the minimal  $SU(3)_c \otimes SU(2)_L \otimes U(1)_Y$  gauge framework. To achieve this, in addition to the Standard Model singlets  $\nu^c$  and  $S$ , we now add a complex scalar singlet  $\sigma$  carrying two units of lepton number. Lepton number symmetry is then spontaneously broken by the vacuum expectation value of  $\sigma$ . The relevant Lagrangian is given by

$$-\mathcal{L} = \sum_{i,j}^3 Y_\nu^{ij} L_i \tilde{\Phi} \nu_j^c + M^{ij} \nu_i^c S_j + Y_S^{ij} \sigma S_i S_j + \text{H.c.} \quad (4.1)$$

After the electroweak and lepton number symmetry breaking the neutrino mass matrix has

the following form

$$\mathcal{M}_\nu = \begin{pmatrix} 0 & m_D & 0 \\ m_D^T & 0 & M \\ 0 & M^T & \mu_S \end{pmatrix} \quad (4.2)$$

where  $m_D = \frac{Y_\nu v_\Phi}{\sqrt{2}}$ ,  $\mu_S = 2 \frac{Y_S v_\sigma}{\sqrt{2}}$  with  $\langle \Phi \rangle = \frac{v_\Phi}{\sqrt{2}}$  and  $\langle \sigma \rangle = \frac{v_\sigma}{\sqrt{2}}$  being the vacuum expectation values (vevs) of the  $\Phi$  and  $\sigma$  fields respectively. Again, within the standard seesaw approximation, the effective neutrino mass is obtained as

$$m_\nu \simeq \frac{v_\Phi^2}{\sqrt{2}} Y_\nu M^{-1} Y_S v_\sigma (M^T)^{-1} Y_\nu^T \quad (4.3)$$

Light neutrino masses of  $\mathcal{O}(0.1)$  eV, are generated for reasonable choices of  $v_\sigma$  and  $M$ , small Yukawa couplings  $Y_S$ , and sizeable  $Y_\nu \sim \mathcal{O}(1)$ .

Turning to the scalar sector, in the presence of the complex scalar singlet  $\sigma$  and doublet  $\Phi$ , the most general potential driving electroweak and lepton number symmetry breaking is given by

$$V = -\mu_\Phi^2 \Phi^\dagger \Phi - \mu_\sigma^2 \sigma^\dagger \sigma + \lambda_\Phi (\Phi^\dagger \Phi)^2 + \lambda_\sigma (\sigma^\dagger \sigma)^2 + \lambda_{\Phi\sigma} (\Phi^\dagger \Phi) (\sigma^\dagger \sigma). \quad (4.4)$$

As already noted, in addition to the  $SU(3)_c \otimes SU(2)_L \otimes U(1)_Y$  gauge invariance,  $V(\Phi, \sigma)$  also has a global  $U(1)$  lepton number symmetry.

This potential is bounded from below if  $\lambda_\sigma$ ,  $\lambda_\Phi$  and  $\lambda_{\Phi\sigma} + 2\sqrt{\lambda_\sigma \lambda_\Phi}$  are all positive, and has a minimum for non-zero vacuum expectation values of both  $\Phi$  and  $\sigma$  provided  $\lambda_\Phi$ ,  $\lambda_\sigma$  and  $4\lambda_\Phi \lambda_\sigma - \lambda_{\Phi\sigma}^2$  are all positive. After the breaking of electroweak and lepton number symmetries, we end up with a physical Goldstone boson, the Majoron  $J$  [18, 19], which is a pure gauge singlet. After symmetry breaking one has, in the unitary gauge,

$$\Phi \rightarrow \frac{1}{\sqrt{2}} \begin{pmatrix} 0 \\ v_\Phi + h' \end{pmatrix}, \quad \sigma \rightarrow \frac{v_\sigma + \sigma' + iJ}{\sqrt{2}}. \quad (4.5)$$

The CP even fields  $h'$  and  $\sigma'$  will mix, so the mass matrix for neutral scalar  $M_{ns}$  is given by

$$M_{ns}^2 = \begin{pmatrix} 2\lambda_\Phi v_\Phi^2 & \lambda_{\Phi\sigma} v_\Phi v_\sigma \\ \lambda_{\Phi\sigma} v_\Phi v_\sigma & 2\lambda_\sigma v_\sigma^2 \end{pmatrix} \quad (4.6)$$

We can diagonalise the above mass matrix to obtain the mass eigenstates  $(h \ H)^T$  through the rotation matrix  $O_R$  as

$$\begin{pmatrix} h \\ H \end{pmatrix} = O_R \begin{pmatrix} h' \\ \sigma' \end{pmatrix} \equiv \begin{pmatrix} \cos \alpha & \sin \alpha \\ -\sin \alpha & \cos \alpha \end{pmatrix} \begin{pmatrix} h' \\ \sigma' \end{pmatrix}, \quad (4.7)$$

Here  $\alpha$  is the CP-even scalar mixing angle, and its range of allowed values is constrained by LHC data [47, 48]. The rotation matrix satisfies

$$O_R M_{ns}^2 O_R^T = \text{diag}(m_h^2, m_H^2) \quad (4.8)$$

where the masses  $m_h, m_H$  of the scalars  $h, H$  respectively, are given by

$$m_h^2 = \lambda_\Phi v_\Phi^2 + \lambda_\sigma v_\sigma^2 - \sqrt{(\lambda_\Phi v_\Phi^2 - \lambda_\sigma v_\sigma^2)^2 + (\lambda_{\Phi\sigma} v v_\sigma)^2} \quad (4.9)$$

$$m_H^2 = \lambda_\Phi v_\Phi^2 + \lambda_\sigma v_\sigma^2 + \sqrt{(\lambda_\Phi v_\Phi^2 - \lambda_\sigma v_\sigma^2)^2 + (\lambda_{\Phi\sigma} v v_\sigma)^2} \quad (4.10)$$

The lighter of these two mass eigenstates  $h$  is identified with the 125 GeV scalar discovered at the LHC [1, 2].

We can use Eqs. (4.9) and (4.10) along with (4.6)-(4.7) to solve for the parameters  $\lambda_\Phi$ ,  $\lambda_\sigma$  and  $\lambda_{\Phi\sigma}$  in terms of physical quantities i.e. masses  $m_h^2$ ,  $m_H^2$  and the mixing angle  $\alpha$  as

$$\lambda_\Phi = \frac{m_h^2 \cos^2 \alpha + m_H^2 \sin^2 \alpha}{2v_\Phi^2}, \quad (4.11)$$

$$\lambda_\sigma = \frac{m_h^2 \sin^2 \alpha + m_H^2 \cos^2 \alpha}{2v_\sigma^2}, \quad (4.12)$$

$$\lambda_{\Phi\sigma} = \frac{(m_h^2 - m_H^2) \sin \alpha \cos \alpha}{v_\Phi v_\sigma}. \quad (4.13)$$

## 5 Vacuum stability in inverse seesaw with majoron

In this section we will explore the consequences of spontaneous breaking of the lepton number symmetry on the stability of the electroweak vacuum. Due to the presence of the scalar  $\sigma$ , the RGE of the  $\Phi$  quartic coupling receives a new 1-loop contribution through the diagram shown in Fig. 7. This “positive” contribution plays a crucial role in counteracting the “negative” contribution coming from the extra fermions of the inverse seesaw model, see Fig. 3.

Vacuum stability in this model can be studied in two different regimes namely i)  $v_\sigma \gg v_\Phi$  and ii)  $v_\sigma \approx \mathcal{O}(v_\Phi)$ . We start with the first possibility. As before, we focus on the missing partner (3, 1, 1) inverse seesaw, other possibilities will be taken up in Section 6.

### 5.1 Case I: $v_\sigma \gg v_\Phi$

In the limit  $v_\sigma \gg v_\Phi$  the heavy CP-even Higgs boson  $H$  almost decouples, with its mass  $m_H$  given as  $m_H \equiv M_H \approx \sqrt{2\lambda_\sigma} v_\sigma$ . Moreover, in this limit small neutrino masses require small  $Y_S$ , so the two heavy singlet fermions  $\nu^c$  and  $S$  form a quasi-Dirac pair with nearly degenerate mass  $M$ . We assume, for simplicity of the analysis, that  $M_H$  and  $M$ , have a common value, so that we deal with just one threshold scale  $\Lambda = M = M_H$ . Below this scale we have an effective theory with the Standard Model structure, supplemented by the Weinberg operator for neutrino mass generation<sup>5</sup>. Thus, below the threshold scale, we need

<sup>5</sup>Note that the majoron  $J$  will also be present in this effective theory. Even though massless or fairly light, it will practically decouple from the Higgs boson, and will not affect vacuum stability.

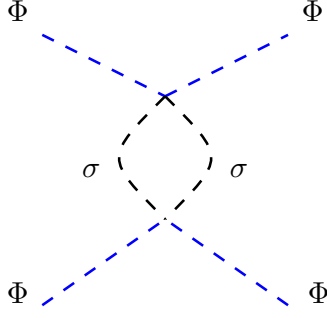


**Figure 7.** One-loop correction to the  $\Phi$  quartic coupling due to its interaction with the singlet  $\sigma$  that drives spontaneous lepton number violation in inverse seesaw models. This diagram leads to a “positive” term in the RGE of the  $\Phi$  quartic coupling, that can overcome the destabilizing effect of the fermions in Fig. 3.

to integrate out  $\sqrt{2}\text{Re}(\sigma)$  at tree-level [49]. As a result, at the scale  $\Lambda$ , there is a tree-level threshold correction which induces a shift in the Higgs quartic coupling,  $\delta\lambda = \frac{\lambda_{\Phi\sigma}^2}{4\lambda_\sigma}$ . This will lead to the following effective Higgs potential below the threshold scale  $\Lambda$

$$V_{\text{eff}} = \lambda'_\Phi \left( \Phi^\dagger \Phi - \frac{v^2}{2} \right)^2, \quad (5.1)$$

where the effective Higgs quartic coupling  $\lambda'_\Phi$  below the threshold scale is defined as

$$\lambda'_\Phi \equiv \lambda_\kappa = \lambda_\Phi - \frac{\lambda_{\Phi\sigma}^2}{4\lambda_\sigma}. \quad (5.2)$$

Here  $\lambda_\kappa$  is the effective quartic coupling for the case of explicit lepton number breaking, see Section 3. The evolution of the Higgs quartic coupling  $\lambda'_\Phi$  in the effective theory is shown in Fig. 8. One can appreciate the jump in the value of the Higgs quartic coupling due to threshold corrections. Since only the dimension-five Weinberg operator runs below the scale  $\Lambda$ , the RG evolution of  $\lambda_{\text{SM}}$  is essentially the same as that of  $\lambda'_\Phi$ . Both are very close to the RG running of  $\lambda_\kappa$  of the effective theory with explicit lepton number breaking. Moreover, at tree-level the numerical value of  $\lambda_\kappa(M_Z)$  and  $\lambda_{\text{SM}}(M_Z)$  is the same, since in both cases one must reproduce the 125 GeV Higgs mass.

Moving on to the full theory at the threshold scale  $\Lambda = M$ , the first thing to note is the impact of threshold corrections, Eq. 5.2. They lead to a positive shift in value of the Higgs quartic coupling above the threshold scale  $\Lambda = M$ , enhancing the chances of keeping  $\lambda_\Phi$  positive [5]. Furthermore, to understand the evolution of  $\lambda_\Phi$  in the full theory above the scale  $\Lambda = M$  one must perform the RG evolution of all parameters. Above the scale  $\Lambda$  one needs to include  $\beta_{\lambda_{\Phi\sigma}}$ ,  $\beta_{\lambda_\sigma}$  and evolve the quartic coupling  $\lambda_\Phi$  using the full RGEs with the matching condition Eq. 5.2 at  $\Lambda$ . In Appendix. B, we give the two-loop RGEs of the full theory.

In Fig. 8 we show the evolution of various couplings in the majoron inverse seesaw model for given benchmark points. We have taken the threshold scale as  $M = M_H = 10$

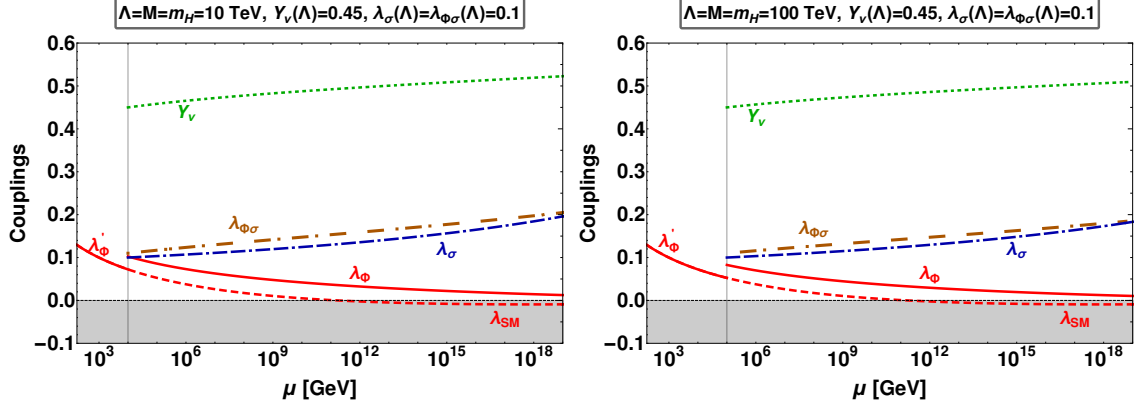


**Figure 8.** The RG evolution of the quartic couplings and right-handed neutrino Yukawa couplings within the Majoron extension of (3,1,1) inverse seesaw scheme. For comparison, we also show the evolution of  $\lambda_{\text{SM}}$  (red-dashed). Here  $\lambda'_\Phi \equiv \lambda_\kappa$  is the effective Higgs quartic coupling below threshold, see Eq. 5.2.

TeV and  $M = M_H = 100$  TeV for the left and right panels, respectively. For the sake of comparison, the initial values of other parameters have been kept the same in both panels. The Yukawa coupling has been fixed at  $Y_\nu = 0.45$ . We have taken  $\lambda_\sigma, \lambda_{\Phi\sigma} = 0.1$  at the scale  $\Lambda$ . The positive shift in the evolution of  $\lambda$  at the threshold scale is coming from the matching condition given in Eq. 5.2. Notice that below threshold the running of  $\lambda'_\Phi$  and  $\lambda_{\text{SM}}$  almost coincide with each other, due to the tiny effective Weinberg operator. Finally, since  $Y_S$  has been taken to be very small, it has no direct impact on vacuum stability.

In summary, it is clear from Fig. 8 that the dynamical variant of the inverse seesaw mechanism can be free from the Higgs vacuum instability problem. This is possible thanks to the positive contribution of the scalar  $\sigma$  both to the threshold corrections, as well as to the RG evolution of the Higgs quartic coupling. These effects are enough to counteract the negative contribution of the new fermions present in inverse seesaw model, even for sizeable Yukawa couplings  $Y_\nu \sim \mathcal{O}(1)$ . These could lead to a plethora of new phenomena [28–41]. Thus, in contrast to the case of inverse seesaw with explicitly broken lepton number, the dynamical variants can have a completely stable Higgs vacuum.

## 5.2 Case II: $v_\sigma = \mathcal{O}(v_\Phi)$

In this case, the mass of the heavy scalar  $m_H$  is of the order of the electroweak scale. Hence we can neglect the small range between  $M_Z$  and  $m_H$ , starting instead with Eq. 4.13, which already includes the threshold effect of Eq. 5.2. Thus in this case only the fermions are integrated out at the threshold scale  $\Lambda = M$ , while all the scalars remain in the resulting theory below threshold. Thus the scalar couplings evolve over a larger range, and have better chance of curing the Higgs vacuum instability problem. Needless to say that, as before, the Higgs vacuum instability can be avoided if the mixed quartic  $\lambda_{\Phi\sigma}$  is sufficiently large,  $\mathcal{O}(0.1)$ . This in turn implies a sizeable mixing  $\alpha \sim \mathcal{O}(0.1)$  between the two CP-even

Higgs bosons.

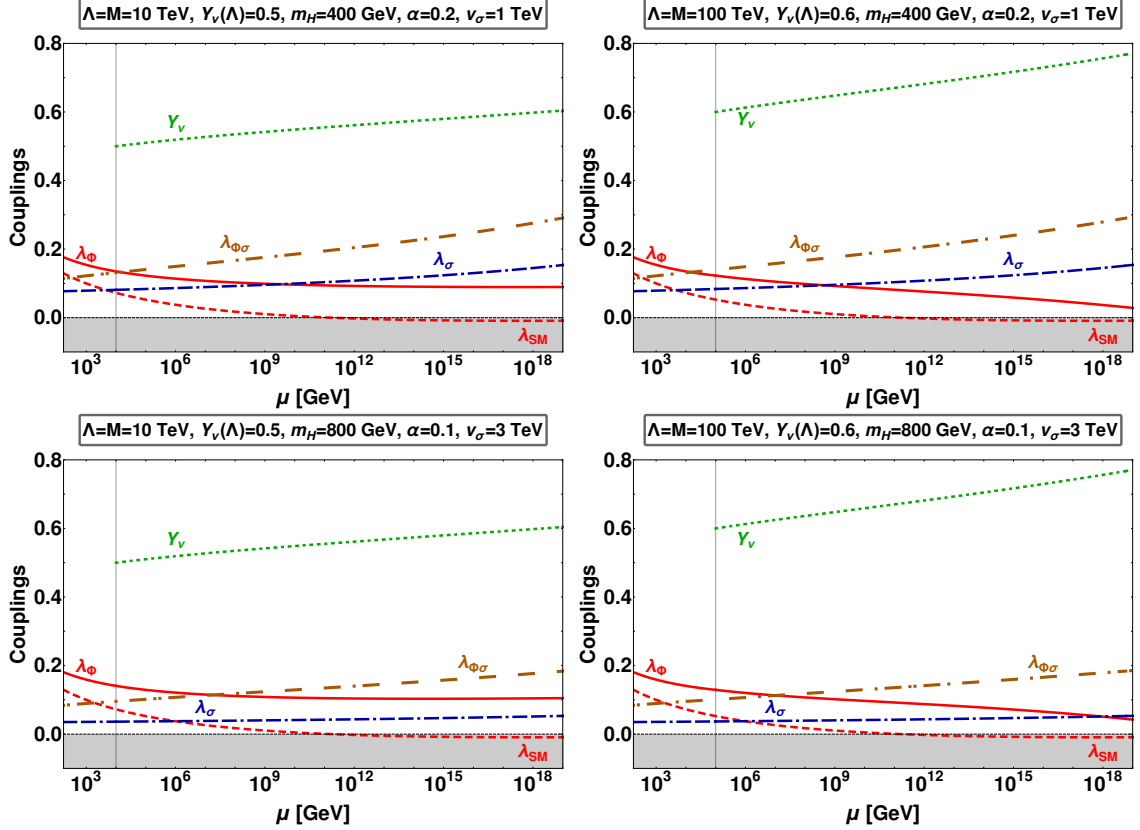


**Figure 9.** Evolution of the quartic couplings and right-handed neutrino Yukawas within the Majoron extension of the missing partner (3,1,1) inverse seesaw scheme. For comparison, the evolution of  $\lambda_{\text{SM}}$  is shown in the red dashed curve. Here only the fermion singlets are integrated out at the threshold scale  $\Lambda = M$ , all scalars are part of the effective theory below threshold, taken as the weak scale.

The evolution of the couplings in this case is shown in Fig. 9. In these plots, we have fixed the singlet neutrino scale  $\Lambda = 10$  TeV in the left panel, and 100 TeV in the right panel. In contrast to the scalar couplings, the Yukawa coupling  $Y_\nu$  starts running only above threshold. Notice that for relatively large mediator scale, the allowed value of  $Y_\nu$  will also be large as there is not enough range, in terms of RGEs evolution, to sizeably alter the  $Y_\nu$ . We found that for large Yukawa couplings,  $Y_\nu \geq 0.7$  (0.8) for threshold scale  $\Lambda = 10$  TeV (100 TeV), respectively, we get either unstable vacuum or non-perturbative dynamics.

Moreover, as shown in Fig. 9, we can have positive  $\lambda_\Phi$ ,  $\lambda_\sigma$  and  $\lambda_{\Phi\sigma}$  all the way up to the Planck scale, even for sizeable Yukawa couplings. We found that for small  $m_H$  the required mixing angle is relatively large, in contrast to the large  $m_H$  case. For small  $\alpha$  or  $m_H$  the potential becomes unbounded from below at high energies. In other words, experimental limits on  $\alpha$ , e.g. coming from the LHC [47, 48], can be used to place a lower limit on the mass  $m_H$ . In Sec. 7 we illustrate the interplay between the vacuum stability restrictions



and the constraints on the invisible width of the Higgs boson that follow from current LHC experiments. There we also note that in order to prevent the existence of Landau poles in the running parameters, the lepton number breaking scale  $v_\sigma$  should not be too small.

## 6 Comparing sequential and missing partner inverse seesaw

For simplicity we have so far only analyzed the explicit and dynamical lepton number breaking within the simplest (3,1,1) missing partner inverse seesaw mechanism. We now compare the stability properties of this minimal construction with those of (3,2,2) and (3,3,3) inverse seesaw mechanisms.

### 6.1 Sequential versus missing partner seesaw: electroweak vacuum stability

As already mentioned, the problem of Higgs vacuum stability only gets worse with the addition of extra fermions. This fact is clearly illustrated in Fig. 10 where we compare the RG evolution of the Higgs quartic coupling  $\lambda$  within the Standard Model (dashed, red) with the (3,  $n$ ,  $n$ ) inverse seesaw completions, with  $n = 1$  (solid, blue),  $n = 2$  (dot-dash, magenta) and  $n = 3$  (dot, green).

In Fig. 10 we have taken the initial Yukawa coupling values in such a way as to facilitate a proper comparison of the different cases. To do this for (3,1,1) case, we have fixed the Yukawa coupling  $|Y_\nu| = 0.4$ . For (3,2,2) and (3,3,3) case, we have taken the diagonal entries of the  $Y_\nu$  matrix to be  $Y_\nu^{ii} = 0.4$ , while all off-diagonal ones,  $Y_\nu^{ij}$  for  $i \neq j$ , were neglected in the RGEs. Clearly one sees how (3,  $n$ ,  $n$ ) inverse seesaw scenarios with  $n > 1$  have worse Higgs vacuum stability properties than the  $n = 1$  case.

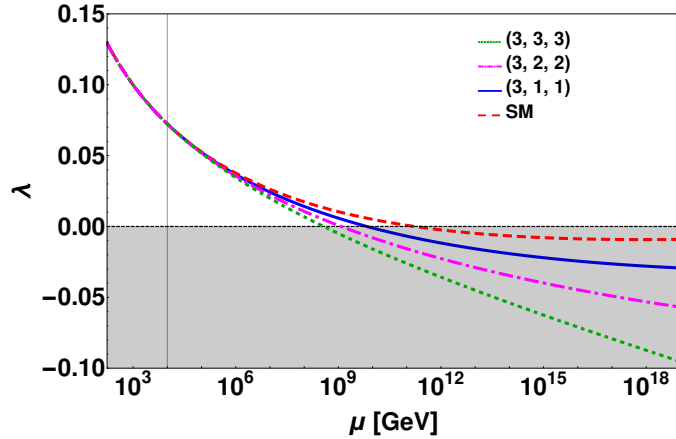


**Figure 10.** Comparing the evolution of the quartic Higgs self-coupling  $\lambda$  in the Standard Model (dashed, red) with various inverse-seesaw extensions with explicit lepton number violation: (3,1,1) denoted in solid (blue), (3,2,2) dot-dashed (magenta) and (3,3,3) dotted (green), see text for details.

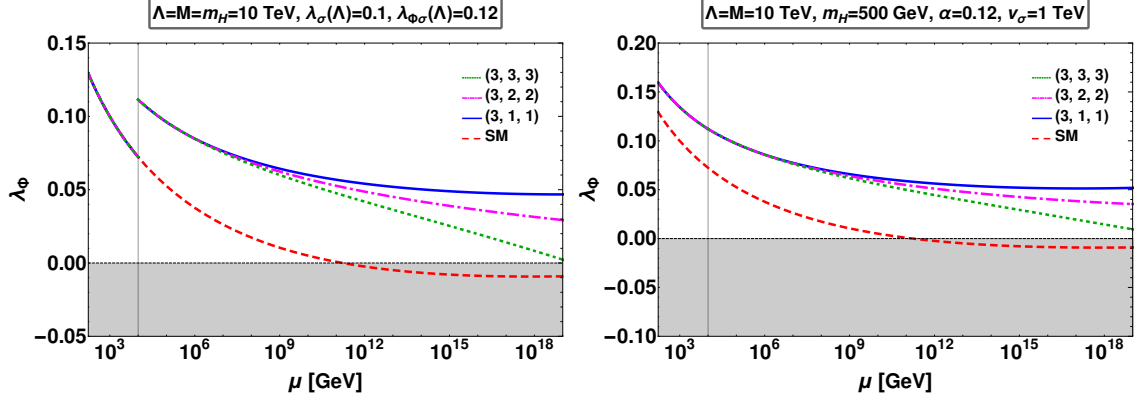


**Figure 11.** Comparing the evolution of the quartic Higgs self-coupling  $\lambda$  in the Standard Model (red dashed) with the majoron inverse seesaw mechanism: the minimal (3,1,1) is denoted in solid (blue), (3,2,2) is dot-dashed (magenta) and (3,3,3) is dotted (green). See text for details.

In Fig. 11, we display our vacuum stability results for the majoron inverse seesaw models. One can compare the Standard Model case (dashed, red) with the (3,1,1) (solid, blue), (3,2,2) (dot-dash, magenta) and (3,3,3) (dot, green) majoron inverse seesaw schemes. As before, to ensure a consistent comparison, we have taken the Yukawa coupling  $|Y_\nu| = 0.4$  for (3,1,1) case, while for the (3,2,2) and (3,3,3) cases, we have taken  $Y_\nu^{ii} = 0.4$  and neglected off-diagonal  $Y_\nu^{ij}$ . In the left panel we have taken the case of  $\Lambda = M = m_H = 10$  TeV. Below threshold we have integrated out the fields  $\sqrt{2}\text{Re}(\sigma)$ ,  $\nu^c$  and  $S$  and included the threshold effects. This leads to the jump in the quartic coupling seen in the figure. In contrast, for the right panel, we have fixed  $v_\sigma = 1$  TeV and  $m_H = 500$  GeV. In this case the scalars are not integrated out and the quartic coupling runs smoothly from electroweak scale till Planck scale.

Fig. 11 clearly illustrates that even for  $n \geq 2$ , we can have a stable electroweak vacuum for adequate choices of  $\alpha$  and  $m_H$ . Indeed, even in the higher (3,2,2) and (3,3,3) majoron inverse seesaw, the positive contribution from the new scalar is enough to overcome the negative contribution from the new fermions of the inverse seesaw. In short, the Higgs vacuum can be kept stable all the way up to the Planck scale even for appreciable Yukawa coupling  $Y_\nu$ .

## 6.2 Sequential versus missing partner seesaw: brief phenomenological discussion

Here we note that neither the explicit nor the dynamical variant of the minimal (3,1,1) inverse seesaw mechanism is phenomenologically realistic. The reason is that (3,1,1) leads to only one massive neutrino (lying say, at the atmospheric scale), hence inconsistent with oscillation data [8]. This minimal scheme is simply the inverse seesaw embedding of the minimum “missing partner” (3,1) seesaw mechanism of Sec.III in Ref. [17]. This lack of the

solar neutrino mass splitting can be avoided by the presence of a complementary radiative mechanism. To implement such “radiative completion” of the minimal scheme one would need to invoke new physics. The latter could be associated, say, to the presence of a dark matter sector [50]. This would provide an elegant theory with a tree-level atmospheric scale, and a radiatively-induced solar neutrino mass scale, very much analogous to the case of the bilinear breaking of R-parity in supersymmetry [51–53].

Alternatively, one can generate non-zero tree-level masses for two neutrinos by going directly to the (3,2,2) “missing partner” seesaw scheme. Again, this would be the inverse-seesaw-analogue of the (3,2) seesaw mechanism in Ref. [17]. Finally, the sequential (3,3,3) inverse seesaw mechanism will generate tree-level masses for all three light neutrinos. Any of these would be totally consistent with neutrino oscillations <sup>6</sup>.

Concerning neutrinoless double beta decay, here lies an important phenomenological difference between the “missing partner” and the “sequential” seesaw mechanism. In the missing partner seesaw there can be no cancellation amongst the individual light-neutrino amplitudes leading to the decay [54] <sup>7</sup>. As a result, there is a lower bound on the neutrinoless double beta decay rates that could be testable in the upcoming generation of searches.

There are other implications of low-scale seesaw schemes, such as our inverse-seesaw, that could be potentially testable in current or upcoming experiments. For example, the associated heavy neutrino mediators could be accessible at high energy experiments such as  $e^+e^-$  collider [28–31], with stringent bounds, e.g. from the Delphi and L3 collaborations [29, 30]. Likewise, they could produce interesting signatures at the LHC [58, 59]. Moreover, these mediators would also induce lepton flavour and leptonic CP violation effects with potentially detectable rates, unsuppressed by the small neutrino masses [32–36]. Finally, since the heavy singlet neutrinos would not take part in oscillations, these could reveal new features associated to unitarity violation in the lepton mixing matrix [37–41]. A dedicated study would be required to scrutinize whether these signatures could be used to distinguish missing partner from sequential seesaw.

## 7 Impact of invisible Higgs decay on the vacuum stability

As we saw above, vacuum stability is often threatened by the violation of the condition  $\lambda_\Phi > 0$ . From the RGE running of  $\lambda_\Phi$  in Eq. B.1 one sees that in order to overcome the destabilizing effect coming from fermions ( $-6y_t^4$  and  $-2\text{Tr}(Y_\nu Y_\nu^\dagger Y_\nu Y_\nu^\dagger)$ ), one needs a relatively large mixed quartic coupling  $\lambda_{\Phi\sigma}$ . This in turn translates into a large mixing angle  $\alpha$  between the  $CP$ -even neutral Higgs bosons  $h$  and  $H$ . We see from Eq. 4.13 that large  $\lambda_{\Phi\sigma}$

---

<sup>6</sup>Modulo, of course, explaining the detailed pattern of mixing angles indicated by the oscillation data [8]. Such a challenging task would require a family symmetry, whose detailed nature is not yet fully understood.

<sup>7</sup>This feature may also be implemented in some radiative schemes of scotogenic type, see e.g. [55–57].

implies smaller mixing angle  $|\sin \alpha|$  for larger  $m_H$  and vice-versa. Within dynamical low-scale seesaw schemes with  $v_\sigma \sim \mathcal{O}(\text{TeV})$ , relatively large mixing angle  $|\sin \alpha|$  is expected. This is in potential conflict with the invisible Higgs decay constraints from LHC.

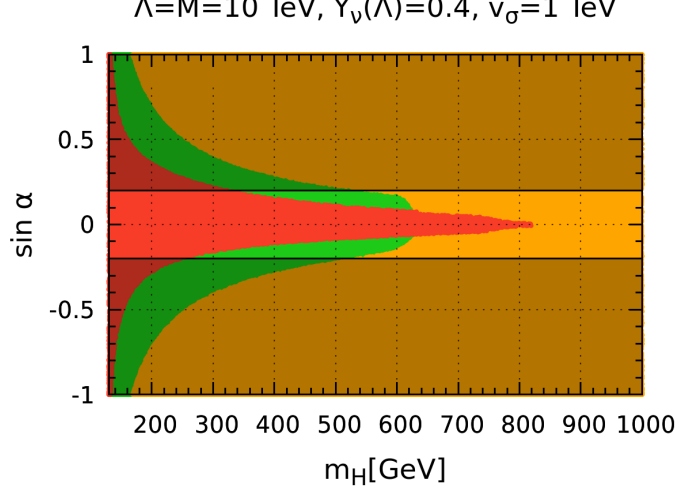


**Figure 12.** Values of  $m_H$  and mixing angle  $\alpha$  leading to a stable potential (green), an unstable potential (red) and non-perturbative dynamics (orange). Here we take the (3,1,1) missing partner majoron inverse seesaw as the reference, with the heavy fermion threshold scale fixed as  $\Lambda = 10$  TeV, Yukawa coupling  $Y_\nu = 0.4$  and  $v_\sigma = 1$  TeV. Within the green region all couplings are perturbative and the vacuum is stable up to the Planck scale. In the red region the potential becomes unbounded from below before the Planck scale. The orange region has nonperturbative couplings (including Landau poles) at energy scales below the Planck scale. The region outside the horizontal band delimited by the black lines is ruled out by the LHC constraints on invisible Higgs decays. More details in text.

Indeed, it has long been noted that models with spontaneous violation of global symmetries such as lepton number at low scales  $v_\sigma \sim \mathcal{O}(\text{TeV})$  lead to sizeable invisible Higgs decays, i.e.  $h \rightarrow JJ$  [23] where  $J$  is the Majoron. The existence of such invisible decays can be probed by the LHC experiments [47, 60, 61]. The tightest bound on invisible Higgs boson decays comes from the CMS experiment at the LHC,  $\text{BR}(h \rightarrow \text{Invisible}) \leq 19\%$  [62]. This upper limit on the invisible Higgs decay sets a tight constraint on  $\lambda_{\Phi\sigma}$  or  $|\sin \alpha|$  for  $m_H > 130$  GeV. For example with  $v_\sigma = 1$  TeV one gets  $|\sin \alpha| < 0.2$  for  $m_H > 130$  GeV.

So far in all of our discussions we have chosen the mixing angle  $|\sin \alpha|$  for fixed  $v_\sigma$  and  $m_H$  in such a way that one has consistency with the CMS constraint on invisible Higgs decay. However, the full parameter space of the model contains regions consistent with vacuum stability but disallowed by the invisible Higgs decay constraints. We illustrate this in Fig. 12 for the (3,1,1) missing partner seesaw with relatively large Yukawa coupling  $Y_\nu = 0.4$ . Fig. 12 shows the values of  $m_H$  and  $\alpha$  for  $v_\sigma = 1$  TeV which lead to either stable/unstable potential or non-perturbative dynamics, as follows:

- **Green Region:** In this region we have a stable vacuum all the way up to the Planck

scale, with all the couplings within the perturbative regime. In our numerical scan these conditions are implemented in following ways:  $0 < \lambda_\Phi(\mu) < 4\pi$ ,  $0 < \lambda_\sigma(\mu) < 4\pi$ ,  $\lambda_{\Phi\sigma}(\mu) + 2\sqrt{\lambda_\Phi(\mu)\lambda_\sigma(\mu)} > 0$ ,  $|\lambda_{\Phi\sigma}(\mu)| < 4\pi$  and  $|Y_\nu(\mu)| < 4\pi$  where  $\mu$  is the running mass scale.

- **Red Region:** In this region the potential becomes unbounded from below at some high energy scale before the Planck scale. The potential is unbounded from below if any (or more) of the following conditions is realised:  $\lambda_\Phi(\mu) \leq 0$ ,  $\lambda_\sigma(\mu) \leq 0$  or  $\lambda_{\Phi\sigma}(\mu) + 2\sqrt{\lambda_\Phi(\mu)\lambda_\sigma(\mu)} \leq 0$ .
- **Orange Region:** Here one or more couplings become non-perturbative below the Planck scale. This happens if any one of the following conditions holds:  $|\lambda_\Phi(\mu)| \geq 4\pi$ ,  $|\lambda_\sigma(\mu)| \geq 4\pi$ ,  $|\lambda_{\Phi\sigma}(\mu)| \geq 4\pi$ ,  $|Y_\nu(\mu)| \geq 4\pi$ . Note that the possibility of Landau poles is also included inside the non-perturbative regions.
- **Collider constraint:** This is the region disallowed due to the LHC restriction on the Higgs invisible decay branching fraction which requires  $\text{BR}(h \rightarrow \text{Invisible}) \leq 19\%$  [62].

From Fig. 12 one sees that for small  $m_H$ , the required mixing angle is large, in order to ensure a stable electroweak vacuum. This is in turn in conflict with the invisible Higgs decay constraints. As a result, one sees that these constraints are complementary to the vacuum consistency requirements of perturbativity and stability. Altogether, these can rule out a large part of the model parameter space.

The above discussion refers to our (3,1,1) majoron inverse seesaw reference case, template for the scoto-seesaw mechanism [50]. One may now wonder how this discussion will change in the higher (3,  $n$ ,  $n$ );  $n \geq 2$  inverse seesaw schemes which do not require a “completion” so as to generate the atmospheric scale. In Fig. 13 we display the results for the (3,2,2) (left panel) and (3,3,3) (right panel) scenarios. As expected, the undesired effect of additional fermions on the stability of the vacuum is clearly visible. Indeed, the unstable red regions in Fig. 13 are larger than in Fig. 12. Likewise, the same effect is seen by comparing the left and right panels of Fig. 13. It is clear from Fig. 12 and Fig. 13 that the allowed parameter space consistent with stability and LHC constraints in the (3,  $n$ ,  $n$ ) seesaw with  $n \geq 2$  is more tightly restricted than in our reference  $n = 1$  case. However we note that, for moderate values of the Yukawa coupling, we still have parameter regions where electroweak breaking is consistent with the LHC measurements. Although in the above we discussed (3,1,1), (3,2,2) and (3,3,3) cases separately, one should note that, in terms of RGE evolution, there is not much difference between them. The corresponding RGEs (see appendix) are the same by replacing  $|Y_\nu|^2$  by  $\text{Tr}(Y_\nu^\dagger Y_\nu)$ . Hence as long as one takes  $|Y_\nu|^2 \approx \text{Tr}(Y_\nu^\dagger Y_\nu)$ , the (3,1,1) and (3,  $n$ ,  $n$ ) with  $n \geq 2$  schemes are effectively the same.

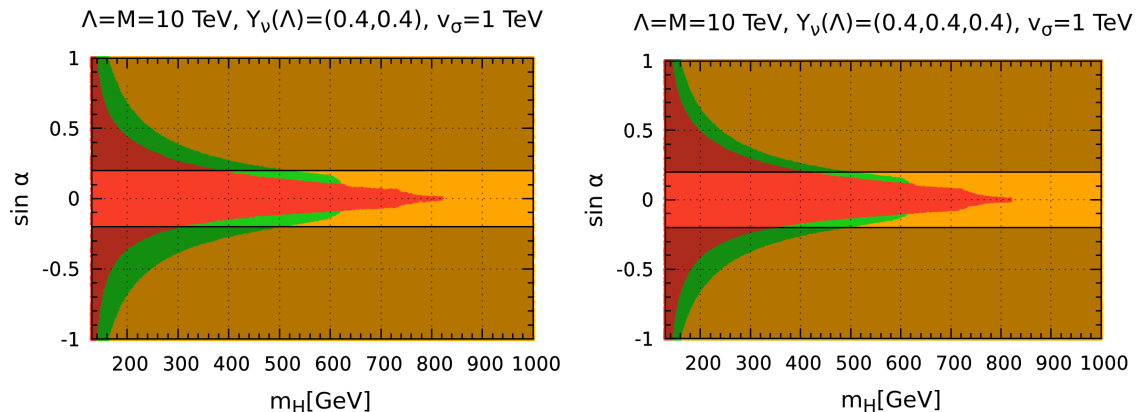


**Figure 13.** Vacuum consistency constraints of Fig. 12 for the case of (3,2,2) (left) and (3,3,3) (right) inverse majoron seesaw mechanism. The diagonal entries of the  $Y_\nu$  matrix are fixed as  $Y_\nu^{ii} = 0.4$ . See text.

Note that the restriction on the mixing angle gets stronger for lower values of  $v_\sigma$  and weakens for higher values of  $v_\sigma$ , disappearing for high enough  $v_\sigma$ . Therefore, the LHC measurements constitute a probe of the lepton number violation scale  $v_\sigma$  associated to neutrino mass generation. Moreover, note that here we have only considered the case when the lighter of the two CP even scalars is identified as the 125 GeV Higgs boson. *A priori*, the possibility that the heavier CP even scalar is the 125 GeV Higgs boson should also be discussed. Finally, in the discussions of Fig. 12 and Fig. 13 we have required vacuum stability and perturbativity all the way up to the Planck scale. This will be an over-requirement, if there is other new physics at play. In that case one should require vacuum stability and perturbativity only up to a lower energy scale, say only up to 100 TeV, thus relaxing the resulting restrictions. All of these issues require a dedicated study, that lies beyond the scope of the present work.

## 8 Conclusions

We have examined the consistency of electroweak symmetry breaking within the inverse seesaw mechanism. We have derived the full two-loop renormalization group equations of the relevant parameters within inverse seesaw schemes, examining both the simplest inverse seesaw with explicit violation of lepton number, as well as the majoron extension of inverse seesaw. The addition of fermion singlets ( $\nu^c$  and  $S$ ) has a destabilizing effect on the running of the Higgs quartic coupling  $\lambda$ . We found that for the inverse seesaw mechanism with sizeable Yukawa coupling  $Y_\nu$  the quartic coupling  $\lambda$  becomes negative much before the Standard Model instability scale  $\sim 10^{10}$  GeV. We have taken as our simplest benchmark neutrino model the “incomplete” (3,1,1) inverse seesaw scheme, as it has the “best” stability properties within this class of seesaw schemes. We compared this reference case, in which only one oscillation scale is generated at tree-level, with the “higher” inverse seesaw

constructions  $(3, n, n)$  with  $n = 2, 3$ , in which other mass scales, such as the atmospheric scale, also arise from the tree-level seesaw mechanism. Our main results on the stability of the electroweak vacuum are summarized in Figs. 4, 8, 9, 10 and 11. We showed how, in contrast to simplest inverse seesaw with explicit lepton number violation, the stability properties improve when this violation is spontaneous, and there is a physical Nambu-Goldstone boson, the majoron. The comparison with LHC restrictions is given in Figs. 12 and 13. We found that the LHC measurements constitute a probe of the lepton number violation scale  $v_\sigma$  associated to neutrino mass generation. Its detailed study, however, needs further investigation. For example, we have assumed the lighter of the two CP even scalars to be the 125 GeV Higgs boson. The alternative intriguing possibility should *a priori* also be considered. We have also required vacuum stability and perturbativity all the way up to the Planck scale. This is clearly an over-requirement, in the presence of additional new physics. The latter could be associated say, to dark matter or to the strong CP problem. In such case one should require vacuum stability and perturbativity only up to a lower intermediate energy scale, thus relaxing the restrictions we have obtained. All of these issues require a dedicated study, that lies beyond the scope of the present work.

## A RGEs: Inverse seesaw

In our work we have used the package SARAH [63] to perform the RG analysis. The  $\beta$  function of a given parameter  $c$  is given by,

$$\mu \frac{dc}{d\mu} \equiv \beta_c = \frac{1}{16\pi^2} \beta_c^{(1)} + \frac{1}{(16\pi^2)^2} \beta_c^{(2)}.$$

where  $\mu$  is the running scale and  $\beta_c^{(1)}$ ,  $\beta_c^{(2)}$  are the one-loop and two-loop RG corrections.

### A.1 Higgs quartic scalar self coupling

The one-loop and two-loop RG corrections to the Higgs quartic self-coupling are given by

$$\begin{aligned} \beta_\lambda^{(1)} = & +\frac{27}{200}g_1^4 + \frac{9}{20}g_1^2g_2^2 + \frac{9}{8}g_2^4 - \frac{9}{5}g_1^2\lambda - 9g_2^2\lambda + 24\lambda^2 + 12\lambda y_t^2 + 4\lambda \text{Tr}(Y_\nu Y_\nu^\dagger) \\ & - 6y_t^4 - 2\text{Tr}(Y_\nu Y_\nu^\dagger Y_\nu Y_\nu^\dagger) \end{aligned} \quad (\text{A.1})$$

$$\begin{aligned} \beta_\lambda^{(2)} = & -\frac{3411}{2000}g_1^6 - \frac{1677}{400}g_1^4g_2^2 - \frac{289}{80}g_1^2g_2^4 + \frac{305}{16}g_2^6 + \frac{1887}{200}g_1^4\lambda + \frac{117}{20}g_1^2g_2^2\lambda - \frac{73}{8}g_2^4\lambda \\ & + \frac{108}{5}g_1^2\lambda^2 + 108g_2^2\lambda^2 - 312\lambda^3 - \frac{171}{100}g_1^4y_t^2 + \frac{63}{10}g_1^2g_2^2y_t^2 - \frac{9}{4}g_2^4y_t^2 + \frac{17}{2}g_1^2\lambda y_t^2 + \frac{45}{2}g_2^2\lambda y_t^2 \\ & + 80g_3^2\lambda y_t^2 - 144\lambda^2 y_t^2 - \frac{9}{100}g_1^4\text{Tr}(Y_\nu Y_\nu^\dagger) - \frac{3}{10}g_1^2g_2^2\text{Tr}(Y_\nu Y_\nu^\dagger) - \frac{3}{4}g_2^4\text{Tr}(Y_\nu Y_\nu^\dagger) \\ & + \frac{3}{2}g_1^2\lambda\text{Tr}(Y_\nu Y_\nu^\dagger) + \frac{15}{2}g_2^2\lambda\text{Tr}(Y_\nu Y_\nu^\dagger) - 48\lambda^2\text{Tr}(Y_\nu Y_\nu^\dagger) - \frac{8}{5}g_1^2y_t^4 - 32g_3^2y_t^4 - 3\lambda y_t^4 \\ & - \lambda\text{Tr}(Y_\nu Y_\nu^\dagger Y_\nu Y_\nu^\dagger) + 30y_t^6 + 10\text{Tr}(Y_\nu Y_\nu^\dagger Y_\nu Y_\nu^\dagger Y_\nu Y_\nu^\dagger) \end{aligned} \quad (\text{A.2})$$

## A.2 Yukawa Couplings

The one-loop and two-loop RG corrections for the most relevant Yukawa couplings in the simplest inverse seesaw model are given by

$$\beta_{Y_\nu}^{(1)} = \frac{3}{2}Y_\nu Y_\nu^\dagger Y_\nu + Y_\nu \left( 3y_t^2 - \frac{9}{20}g_1^2 - \frac{9}{4}g_2^2 + \text{Tr}(Y_\nu Y_\nu^\dagger) \right) \quad (\text{A.3})$$

$$\beta_{Y_\nu}^{(2)} = \frac{1}{80} \left( 279g_1^2 Y_\nu Y_\nu^\dagger Y_\nu + 675g_2^2 Y_\nu Y_\nu^\dagger Y_\nu - 960\lambda Y_\nu Y_\nu^\dagger Y_\nu + 120Y_\nu Y_\nu^\dagger Y_\nu Y_\nu^\dagger Y_\nu - 540Y_\nu Y_\nu^\dagger Y_\nu y_t^2 \right. \\ \left. - 180Y_\nu Y_\nu^\dagger Y_\nu \text{Tr}(Y_\nu Y_\nu^\dagger) + 2Y_\nu \left( 21g_1^4 - 54g_1^2 g_2^2 - 230g_2^4 + 240\lambda^2 + 85g_1^2 y_t^2 + 225g_2^2 y_t^2 \right. \right. \\ \left. \left. + 800g_3^2 y_t^2 + 15g_1^2 \text{Tr}(Y_\nu Y_\nu^\dagger) + 75g_2^2 \text{Tr}(Y_\nu Y_\nu^\dagger) - 270y_t^4 - 90\text{Tr}(Y_\nu Y_\nu^\dagger Y_\nu Y_\nu^\dagger) \right) \right) \quad (\text{A.4})$$

$$\beta_{y_t}^{(1)} = \frac{3}{2}y_t^3 + y_t \left( 3y_t^2 - 8g_3^2 - \frac{17}{20}g_1^2 - \frac{9}{4}g_2^2 + \text{Tr}(Y_\nu Y_\nu^\dagger) \right) \quad (\text{A.5})$$

$$\beta_{y_t}^{(2)} = +\frac{1}{80} \left( 120y_t^5 + y_t^3 \left( 1280g_3^2 - 180\text{Tr}(Y_\nu Y_\nu^\dagger) + 223g_1^2 - 540y_t^2 + 675g_2^2 - 960\lambda \right) \right. \\ \left. + y_t \left( \frac{1187}{600}g_1^4 - \frac{9}{20}g_1^2 g_2^2 - \frac{23}{4}g_2^4 + \frac{19}{15}g_1^2 g_3^2 + 9g_2^2 g_3^2 - 108g_3^4 + 6\lambda^2 + \frac{17}{8}g_1^2 y_t^2 + \frac{45}{8}g_2^2 y_t^2 \right. \right. \\ \left. \left. + 20g_3^2 y_t^2 + \frac{3}{8}g_1^2 \text{Tr}(Y_\nu Y_\nu^\dagger) + \frac{15}{8}g_2^2 \text{Tr}(Y_\nu Y_\nu^\dagger) - \frac{27}{4}y_t^4 - \frac{9}{4}\text{Tr}(Y_\nu Y_\nu^\dagger Y_\nu Y_\nu^\dagger) \right) \right) \quad (\text{A.6})$$

## B RGEs: Inverse seesaw with majoron

In the presence of the majoron the one- and two-loop RG corrections for the quartic scalar couplings in the inverse seesaw model are modified to

### B.1 Quartic scalar couplings

$$\beta_{\lambda_\Phi}^{(1)} = +\frac{27}{200}g_1^4 + \frac{9}{20}g_1^2 g_2^2 + \frac{9}{8}g_2^4 + \lambda_{\Phi\sigma}^2 - \frac{9}{5}g_1^2 \lambda_\Phi - 9g_2^2 \lambda_\Phi + 24\lambda_\Phi^2 + 12\lambda_\Phi y_t^2 + 4\lambda_\Phi \text{Tr}(Y_\nu Y_\nu^\dagger) - 6y_t^4 \\ - 2\text{Tr}(Y_\nu Y_\nu^\dagger Y_\nu Y_\nu^\dagger) \quad (\text{B.1})$$

$$\beta_{\lambda_\Phi}^{(2)} = -\frac{3411}{2000}g_1^6 - \frac{1677}{400}g_1^4 g_2^2 - \frac{289}{80}g_1^2 g_2^4 + \frac{305}{16}g_2^6 - 4\lambda_{\Phi\sigma}^3 + \frac{1887}{200}g_1^4 \lambda_\Phi + \frac{117}{20}g_1^2 g_2^2 \lambda_\Phi - \frac{73}{8}g_2^4 \lambda_\Phi \\ - 10\lambda_{\Phi\sigma}^2 \lambda_\Phi + \frac{108}{5}g_1^2 \lambda_\Phi^2 + 108g_2^2 \lambda_\Phi^2 - 312\lambda_\Phi^3 - 4\lambda_{\Phi\sigma}^2 \text{Tr}(Y_S Y_S^*) - \frac{171}{100}g_1^4 y_t^2 + \frac{63}{10}g_1^2 g_2^2 y_t^2 \\ - \frac{9}{4}g_2^4 y_t^2 + \frac{17}{2}g_1^2 \lambda_\Phi y_t^2 + \frac{45}{2}g_2^2 \lambda_\Phi y_t^2 + 80g_3^2 \lambda_\Phi y_t^2 - 144\lambda_\Phi^2 y_t^2 - \frac{9}{100}g_1^4 \text{Tr}(Y_\nu Y_\nu^\dagger) \\ - \frac{3}{10}g_1^2 g_2^2 \text{Tr}(Y_\nu Y_\nu^\dagger) - \frac{3}{4}g_2^4 \text{Tr}(Y_\nu Y_\nu^\dagger) + \frac{3}{2}g_1^2 \lambda_\Phi \text{Tr}(Y_\nu Y_\nu^\dagger) + \frac{15}{2}g_2^2 \lambda_\Phi \text{Tr}(Y_\nu Y_\nu^\dagger) - 48\lambda_\Phi^2 \text{Tr}(Y_\nu Y_\nu^\dagger) \\ - \frac{8}{5}g_1^2 y_t^4 - 32g_3^2 y_t^4 - 3\lambda_\Phi y_t^4 - \lambda_\Phi \text{Tr}(Y_\nu Y_\nu^\dagger Y_\nu Y_\nu^\dagger) + 30y_t^6 + 10\text{Tr}(Y_\nu Y_\nu^\dagger Y_\nu Y_\nu^\dagger Y_\nu Y_\nu^\dagger) \\ \beta_{\lambda_{\Phi\sigma}}^{(1)} = \frac{1}{10}\lambda_{\Phi\sigma} \left( -9g_1^2 - 45g_2^2 + 40\lambda_{\Phi\sigma} + 80\lambda_\sigma + 120\lambda_\Phi + 40\text{Tr}(Y_S Y_S^*) + 60y_t^2 + 20\text{Tr}(Y_\nu Y_\nu^\dagger) \right) \quad (\text{B.3})$$



$$\begin{aligned}
\beta_{\lambda_{\Phi\sigma}}^{(2)} = & +\frac{1671}{400}g_1^4\lambda_{\Phi\sigma} + \frac{9}{8}g_1^2g_2^2\lambda_{\Phi\sigma} - \frac{145}{16}g_2^4\lambda_{\Phi\sigma} + \frac{3}{5}g_1^2\lambda_{\Phi\sigma}^2 + 3g_2^2\lambda_{\Phi\sigma}^2 - 11\lambda_{\Phi\sigma}^3 - 48\lambda_{\Phi\sigma}^2\lambda_\sigma \\
& - 40\lambda_{\Phi\sigma}\lambda_\sigma^2 + \frac{72}{5}g_1^2\lambda_{\Phi\sigma}\lambda_\Phi + 72g_2^2\lambda_{\Phi\sigma}\lambda_\Phi - 72\lambda_{\Phi\sigma}^2\lambda - 60\lambda_{\Phi\sigma}\lambda_\Phi^2 - 8\lambda_{\Phi\sigma}^2\text{Tr}(Y_S Y_S^*) \\
& - 32\lambda_{\Phi\sigma}\lambda_\sigma\text{Tr}(Y_S Y_S^*) + \frac{17}{4}g_1^2\lambda_{\Phi\sigma}y_t^2 + \frac{45}{4}g_2^2\lambda_{\Phi\sigma}y_t^2 + 40g_3^2\lambda_{\Phi\sigma}y_t^2 - 12\lambda_{\Phi\sigma}^2y_t^2 \\
& - 72\lambda_{\Phi\sigma}\lambda_\Phi y_t^2 + \frac{3}{4}g_1^2\lambda_{\Phi\sigma}\text{Tr}(Y_\nu Y_\nu^\dagger) + \frac{15}{4}g_2^2\lambda_{\Phi\sigma}\text{Tr}(Y_\nu Y_\nu^\dagger) - 4\lambda_{\Phi\sigma}^2\text{Tr}(Y_\nu Y_\nu^\dagger) \\
& - 24\lambda_{\Phi\sigma}\lambda_\Phi\text{Tr}(Y_\nu Y_\nu^\dagger) - 24\lambda_{\Phi\sigma}\text{Tr}(Y_S Y_S^* Y_S Y_S^*) - \frac{27}{2}\lambda_{\Phi\sigma}y_t^4 - \frac{9}{2}\lambda_{\Phi\sigma}\text{Tr}(Y_\nu Y_\nu^\dagger Y_\nu Y_\nu^\dagger)
\end{aligned} \tag{B.4}$$

$$\beta_{\lambda_\sigma}^{(1)} = 2\left(10\lambda_\sigma^2 + 4\lambda_\sigma\text{Tr}(Y_S Y_S^*) - 8\text{Tr}(Y_S Y_S^* Y_S Y_S^*) + \lambda_{\Phi\sigma}^2\right) \tag{B.5}$$

$$\begin{aligned}
\beta_{\lambda_\sigma}^{(2)} = & +\frac{12}{5}g_1^2\lambda_{\Phi\sigma}^2 + 12g_2^2\lambda_{\Phi\sigma}^2 - 8\lambda_{\Phi\sigma}^3 - 20\lambda_{\Phi\sigma}^2\lambda_\sigma - 240\lambda_\sigma^3 - 80\lambda_\sigma^2\text{Tr}(Y_S Y_S^*) - 12\lambda_{\Phi\sigma}^2y_t^2 \\
& - 4\lambda_{\Phi\sigma}^2\text{Tr}(Y_\nu Y_\nu^\dagger) + 16\lambda_\sigma\text{Tr}(Y_S Y_S^* Y_S Y_S^*) + 256\text{Tr}(Y_S Y_S^* Y_S Y_S^* Y_S Y_S^*)
\end{aligned} \tag{B.6}$$

## B.2 Yukawa Couplings

Likewise, in the presence of the majoron the one- and two-loop RG corrections for the Yukawas in the inverse seesaw model are modified to

$$\beta_{Y_\nu}^{(1)} = \frac{3}{2}Y_\nu Y_\nu^\dagger Y_\nu + Y_\nu\left(3y_t^2 - \frac{9}{20}g_1^2 - \frac{9}{4}g_2^2 + \text{Tr}(Y_\nu Y_\nu^\dagger)\right) \tag{B.7}$$

$$\begin{aligned}
\beta_{Y_\nu}^{(2)} = & \frac{1}{80}\left(279g_1^2Y_\nu Y_\nu^\dagger Y_\nu + 675g_2^2Y_\nu Y_\nu^\dagger Y_\nu - 960\lambda_\Phi Y_\nu Y_\nu^\dagger Y_\nu + 120Y_\nu Y_\nu^\dagger Y_\nu Y_\nu^\dagger Y_\nu - 540Y_\nu Y_\nu^\dagger Y_\nu y_t^2\right. \\
& - 180Y_\nu Y_\nu^\dagger Y_\nu\text{Tr}(Y_\nu Y_\nu^\dagger) + 2Y_\nu\left(21g_1^4 - 54g_1^2g_2^2 - 230g_2^4 + 20\lambda_{\Phi\sigma}^2 + 240\lambda_\Phi^2 + 85g_1^2y_t^2\right. \\
& \left. + 225g_2^2y_t^2 + 800g_3^2y_t^2 + 15g_1^2\text{Tr}(Y_\nu Y_\nu^\dagger) + 75g_2^2\text{Tr}(Y_\nu Y_\nu^\dagger) - 270y_t^4 - 90\text{Tr}(Y_\nu Y_\nu^\dagger Y_\nu Y_\nu^\dagger)\right)
\end{aligned} \tag{B.8}$$

$$\beta_{y_t}^{(1)} = \frac{3}{2}y_t^3 + y_t\left(3y_t^2 - 8g_3^2 - \frac{17}{20}g_1^2 - \frac{9}{4}g_2^2 + \text{Tr}(Y_\nu Y_\nu^\dagger)\right) \tag{B.9}$$

$$\begin{aligned}
\beta_{y_t}^{(2)} = & +\frac{1}{80}\left(120y_t^5 + y_t^3\left(1280g_3^2 - 180\text{Tr}(Y_\nu Y_\nu^\dagger) + 223g_1^2 - 540y_t^2 + 675g_2^2 - 960\lambda_\Phi\right)\right. \\
& \left.+ y_t\left(\frac{1187}{600}g_1^4 - \frac{9}{20}g_1^2g_2^2 - \frac{23}{4}g_2^4 + \frac{19}{15}g_1^2g_3^2 + 9g_2^2g_3^2 - 108g_3^4 + \frac{1}{2}\lambda_{\Phi\sigma}^2 + 6\lambda_\Phi^2 + \frac{17}{8}g_1^2y_t^2\right.\right.
\end{aligned} \tag{B.10}$$

$$\left. + \frac{45}{8}g_2^2y_t^2 + 20g_3^2y_t^2 + \frac{3}{8}g_1^2\text{Tr}(Y_\nu Y_\nu^\dagger) + \frac{15}{8}g_2^2\text{Tr}(Y_\nu Y_\nu^\dagger) - \frac{27}{4}y_t^4 - \frac{9}{4}\text{Tr}(Y_\nu Y_\nu^\dagger Y_\nu Y_\nu^\dagger)\right)$$

$$\beta_{Y_S}^{(1)} = 2Y_S\text{Tr}(Y_S Y_S^*) + 4Y_S Y_S^* Y_S \tag{B.11}$$

$$\begin{aligned}
\beta_{Y_S}^{(2)} = & 28Y_S Y_S^* Y_S Y_S^* Y_S - 4Y_S Y_S^* Y_S\left(3\text{Tr}(Y_S Y_S^*) + 8\lambda_\sigma\right) + Y_S\left(-12\text{Tr}(Y_S Y_S^* Y_S Y_S^*)\right. \\
& \left.+ 4\lambda_\sigma^2 + \lambda_{\Phi\sigma}^2\right)
\end{aligned} \tag{B.12}$$

## Acknowledgments

This work is supported by the Spanish grant FPA2017-85216-P (AEI/FEDER, UE), PROMETEO/2018/165 (Generalitat Valenciana), Fundação para a Ciência e a Tecnologia (FCT, Portugal) under project CERN/FIS-PAR/0004/2019, and the Spanish Red Consolider MultiDark FPA2017-90566-REDC.

## References

- [1] ATLAS collaboration, *Observation of a new particle in the search for the Standard Model Higgs boson with the ATLAS detector at the LHC*, *Phys. Lett. B* **716** (2012) 1 [[1207.7214](#)].
- [2] CMS collaboration, *Observation of a New Boson at a Mass of 125 GeV with the CMS Experiment at the LHC*, *Phys. Lett. B* **716** (2012) 30 [[1207.7235](#)].
- [3] PARTICLE DATA GROUP collaboration, *Review of Particle Physics*, *Phys. Rev.* **D98** (2018) 030001.
- [4] D. Buttazzo, G. Degrassi, P.P. Giardino, G.F. Giudice, F. Sala, A. Salvio et al., *Investigating the near-criticality of the Higgs boson*, *JHEP* **12** (2013) 089 [[1307.3536](#)].
- [5] S. Mandal, R. Srivastava and J.W.F. Valle, *Consistency of the dynamical high-scale type-I seesaw mechanism*, *Phys. Rev. D* **101** (2020) 115030 [[1903.03631](#)].
- [6] G. Degrassi, S. Di Vita, J. Elias-Miro, J.R. Espinosa, G.F. Giudice, G. Isidori et al., *Higgs mass and vacuum stability in the Standard Model at NNLO*, *JHEP* **08** (2012) 098 [[1205.6497](#)].
- [7] S. Alekhin, A. Djouadi and S. Moch, *The top quark and Higgs boson masses and the stability of the electroweak vacuum*, *Phys.Lett.* **B716** (2012) 214 [[1207.0980](#)].
- [8] P. de Salas et al., *2020 Global reassessment of the neutrino oscillation picture*, [2006.11237](#).
- [9] S. Khan, S. Goswami and S. Roy, *Vacuum Stability constraints on the minimal singlet TeV Seesaw Model*, *Phys.Rev.* **D89** (2014) 073021 [[1212.3694](#)].
- [10] W. Rodejohann and H. Zhang, *Impact of massive neutrinos on the Higgs self-coupling and electroweak vacuum stability*, *JHEP* **06** (2012) 022 [[1203.3825](#)].
- [11] C. Bonilla, R.M. Fonseca and J.W.F. Valle, *Vacuum stability with spontaneous violation of lepton number*, *Phys. Lett.* **B756** (2016) 345 [[1506.04031](#)].
- [12] L. Delle Rose, C. Marzo and A. Urbano, *On the stability of the electroweak vacuum in the presence of low-scale seesaw models*, *JHEP* **1512** (2015) 050 [[1506.03360](#)].
- [13] M. Lindner, H.H. Patel and B. Radovčić, *Electroweak Absolute, Meta-, and Thermal Stability in Neutrino Mass Models*, *Phys.Rev.* **D93** (2016) 073005 [[1511.06215](#)].
- [14] J.N. Ng and A. de la Puente, *Electroweak Vacuum Stability and the Seesaw Mechanism Revisited*, *Eur. Phys. J.* **C76** (2016) 122 [[1510.00742](#)].
- [15] G. Bambhaniya, P. Bhupal Dev, S. Goswami, S. Khan and W. Rodejohann, *Naturalness, Vacuum Stability and Leptogenesis in the Minimal Seesaw Model*, *Phys.Rev.* **D95** (2017) 095016 [[1611.03827](#)].

- [16] I. Garg, S. Goswami, K. Vishnudath and N. Khan, *Electroweak vacuum stability in presence of singlet scalar dark matter in TeV scale seesaw models*, *Phys.Rev.* **D96** (2017) 055020 [[1706.08851](#)].
- [17] J. Schechter and J.W.F. Valle, *Neutrino Masses in  $SU(2) \otimes U(1)$  Theories*, *Phys.Rev.* **D22** (1980) 2227.
- [18] Y. Chikashige, R.N. Mohapatra and R.D. Peccei, *Are There Real Goldstone Bosons Associated with Broken Lepton Number?*, *Phys. Lett.* **98B** (1981) 265.
- [19] J. Schechter and J.W.F. Valle, *Neutrino Decay and Spontaneous Violation of Lepton Number*, *Phys. Rev.* **D25** (1982) 774.
- [20] S.M. Boucenna, S. Morisi and J.W. Valle, *The low-scale approach to neutrino masses*, *Adv.High Energy Phys.* **2014** (2014) 831598 [[1404.3751](#)].
- [21] R.N. Mohapatra and J.W.F. Valle, *Neutrino Mass and Baryon Number Nonconservation in Superstring Models*, *Phys. Rev.* **D34** (1986) 1642.
- [22] M. Gonzalez-Garcia and J.W.F. Valle, *Fast Decaying Neutrinos and Observable Flavor Violation in a New Class of Majoron Models*, *Phys.Lett.* **B216** (1989) 360.
- [23] A.S. Joshipura and J. Valle, *Invisible Higgs decays and neutrino physics*, *Nucl.Phys.* **B397** (1993) 105.
- [24] F. Bazzocchi et al., *Calculable inverse-seesaw neutrino masses in supersymmetry*, *Phys.Rev.* **D81** (2010) 051701 [[0907.1262](#)].
- [25] A. Cárcamo Hernández et al., *Neutrino predictions from a left-right symmetric flavored extension of the standard model*, *JHEP* **1902** (2019) 065 [[1811.03018](#)].
- [26] N. Rojas, R. Srivastava and J.W. Valle, *Scotogenic origin of the Inverse Seesaw Mechanism*, [1907.07728](#).
- [27] J.W.F. Valle, *Neutrinoless Double Beta Decay With Quasi Dirac Neutrinos*, *Phys.Rev.* **D27** (1983) 1672.
- [28] M. Dittmar et al., *Production Mechanisms and Signatures of Isosinglet Neutral Heavy Leptons in  $Z^0$  Decays*, *Nucl.Phys.* **B332** (1990) 1.
- [29] DELPHI collaboration, *Search for neutral heavy leptons produced in Z decays*, *Z.Phys.* **C74** (1997) 57.
- [30] L3 collaboration, *Search for heavy isosinglet neutrinos in  $e^+e^-$  annihilation at 130-GeV less than  $S^{(1/2)}$  less than 189-GeV*, *Phys.Lett.* **B461** (1999) 397.
- [31] Y. Cai, T. Han, T. Li and R. Ruiz, *Lepton Number Violation: Seesaw Models and Their Collider Tests*, *Front.in Phys.* **6** (2018) 40 [[1711.02180](#)].
- [32] J. Bernabeu, A. Santamaria, J. Vidal, A. Mendez and J.W.F. Valle, *Lepton Flavor Nonconservation at High-Energies in a Superstring Inspired Standard Model*, *Phys.Lett.* **B187** (1987) 303.
- [33] G. Branco, M. Rebelo and J.W.F. Valle, *Leptonic CP Violation With Massless Neutrinos*, *Phys.Lett.* **B225** (1989) 385.

- [34] N. Rius and J.W.F. Valle, *Leptonic CP Violating Asymmetries in  $Z^0$  Decays*, *Phys.Lett.* **B246** (1990) 249.
- [35] F. Deppisch and J.W.F. Valle, *Enhanced lepton flavor violation in the supersymmetric inverse seesaw model*, *Phys.Rev.* **D72** (2005) 036001.
- [36] F. Deppisch, T. Kosmas and J.W.F. Valle, *Enhanced  $\mu^- \rightarrow e^-$  conversion in nuclei in the inverse seesaw model*, *Nucl.Phys.* **B752** (2006) 80.
- [37] J.W.F. Valle, *Resonant Oscillations of Massless Neutrinos in Matter*, *Phys.Lett.* **B199** (1987) 432.
- [38] H. Nunokawa, Y. Qian, A. Rossi and J.W.F. Valle, *Resonant conversion of massless neutrinos in supernovae*, *Phys.Rev.* **D54** (1996) 4356.
- [39] S. Antusch, C. Biggio, E. Fernandez-Martinez, M. Gavela and J. Lopez-Pavon, *Unitarity of the Leptonic Mixing Matrix*, *JHEP* **0610** (2006) 084.
- [40] O. Miranda and J.W.F. Valle, *Neutrino oscillations and the seesaw origin of neutrino mass*, *Nucl.Phys.* **B908** (2016) 436 [[1602.00864](#)].
- [41] F. Escribuela et al., *On the description of nonunitary neutrino mixing*, *Phys.Rev.* **D92** (2015) 053009 [[1503.08879](#)].
- [42] A. Abada, G. Arcadi and M. Lucente, *Dark Matter in the minimal Inverse Seesaw mechanism*, *JCAP* **10** (2014) 001 [[1406.6556](#)].
- [43] S. Weinberg, *Baryon and Lepton Nonconserving Processes*, *Phys. Rev. Lett.* **43** (1979) 1566.
- [44] P.H. Chankowski et al., *Neutrino unification*, *Phys. Rev. Lett.* **86** (2001) 3488 [[hep-ph/0011150](#)].
- [45] S. Antusch, J. Kersten, M. Lindner and M. Ratz, *Neutrino mass matrix running for nondegenerate seesaw scales*, *Phys. Lett. B* **538** (2002) 87 [[hep-ph/0203233](#)].
- [46] J. Bergstrom, T. Ohlsson and H. Zhang, *Threshold effects on renormalization group running of neutrino parameters in the low-scale seesaw model*, *Phys. Lett. B* **698** (2011) 297 [[1009.2762](#)].
- [47] C. Bonilla, J.W.F. Valle and J.C. Romão, *Neutrino mass and invisible Higgs decays at the LHC*, *Phys. Rev. D* **91** (2015) 113015 [[1502.01649](#)].
- [48] ATLAS collaboration, *Search for Invisible Decays of a Higgs Boson Produced in Association with a Z Boson in ATLAS*, *Phys. Rev. Lett.* **112** (2014) 201802 [[1402.3244](#)].
- [49] J. Elias-Miro, J.R. Espinosa, G.F. Giudice, H.M. Lee and A. Strumia, *Stabilization of the Electroweak Vacuum by a Scalar Threshold Effect*, *JHEP* **06** (2012) 031 [[1203.0237](#)].
- [50] N. Rojas, R. Srivastava and J.W. Valle, *Simplest Scoto-Seesaw Mechanism*, *Phys.Lett.* **B789** (2019) 132 [[1807.11447](#)].
- [51] M.A. Diaz, J.C. Romao and J.W.F. Valle, *Minimal supergravity with R-parity breaking*, *Nucl.Phys.* **B524** (1998) 23.
- [52] M. Hirsch et al., *Neutrino masses and mixings from supersymmetry with bilinear R parity*

- violation: A Theory for solar and atmospheric neutrino oscillations, *Phys.Rev.* **D62** (2000) 113008.
- [53] M.A. Diaz et al., *Solar neutrino masses and mixing from bilinear R parity broken supersymmetry: Analytical versus numerical results*, *Phys.Rev.* **D68** (2003) 013009.
  - [54] J.W.F. Valle, *Neutrino physics outlook*, in *Closing talk at The 21st international workshop on neutrinos from accelerators (NuFact2019)*, August 26 - August 31, 2019, Daegu, Korea , 2020 [2001.03016].
  - [55] M. Reig et al., *Bound-state dark matter with Majorana neutrinos*, *Phys.Lett.* **B790** (2019) 303 [1806.09977].
  - [56] J. Leite et al., *A theory for scotogenic dark matter stabilised by residual gauge symmetry*, *Phys.Lett.* **B802** (2020) 135254 [1909.06386].
  - [57] I.M. Ávila et al., *Minimalistic scotogenic scalar dark matter*, 1910.08422.
  - [58] F.F. Deppisch, P. Bhupal Dev and A. Pilaftsis, *Neutrinos and Collider Physics*, *New J.Phys.* **17** (2015) 075019 [1502.06541].
  - [59] CMS collaboration, *Search for heavy neutral leptons in events with three charged leptons in proton-proton collisions at  $\sqrt{s} = 13$  TeV*, *Phys.Rev.Lett.* **120** (2018) 221801 [1802.02965].
  - [60] C. Bonilla, J.C. Romão and J.W.F. Valle, *Electroweak breaking and neutrino mass: “invisible” Higgs decays at the LHC (type II seesaw)*, *New J. Phys.* **18** (2016) 033033 [1511.07351].
  - [61] D. Fontes, J.C. Romao and J.W. Valle, *Electroweak Breaking and Higgs Boson Profile in the Simplest Linear Seesaw Model*, *JHEP* **10** (2019) 245 [1908.09587].
  - [62] CMS collaboration, *Search for invisible decays of a Higgs boson produced through vector boson fusion in proton-proton collisions at  $\sqrt{s} = 13$  TeV*, *Phys. Lett. B* **793** (2019) 520 [1809.05937].
  - [63] F. Staub, *Exploring new models in all detail with SARAH*, *Adv. High Energy Phys.* **2015** (2015) 840780 [1503.04200].